J. Fluid Mech. (1996), vol. 319, pp. 353–385

A Lagrangian dynamic subgrid-scale model of turbulence

By CHARLES MENEVEAU[1], THOMAS S. LUND[2] AND WILLIAM H. CABOT[2]

[1] The Johns Hopkins University, Baltimore, MD 21218, USA

[2] Center for Turbulence Research, Stanford University, Stanford, CA 94305, USA

(Received 30 January 1995 and in revised form 26 March 1996)

The dynamic model for large-eddy simulation of turbulence samples information from the resolved velocity field in order to optimize subgrid-scale model coefficients. When the method is used in conjunction with the Smagorinsky eddy-viscosity model, and the sampling process is formulated in a spatially local fashion, the resulting coefficient field is highly variable and contains a significant fraction of negative values. Negative eddy viscosity leads to computational instability and as a result the model is always augmented with a stabilization mechanism. In most applications the model is stabilized by averaging the relevant equations over directions of statistical homogeneity. While this approach is effective, and is consistent with the statistical basis underlying the eddy-viscosity model, it is not applicable to complex-geometry inhomogeneous flows. Existing local formulations, intended for inhomogeneous flows, are most commonly stabilized by artificially constraining the coefficient to be positive. In this paper we introduce a new dynamic model formulation, that combines advantages of the statistical and local approaches. We propose to accumulate the required averages over flow pathlines rather than over directions of statistical homogeneity. This procedure allows the application of the dynamic model *with averaging* to inhomogeneous flows in complex geometries. We analyse direct numerical simulation data to document the effects of such averaging on the Smagorinsky coefficient. The characteristic Lagrangian time scale over which the averaging is performed is chosen based on measurements of the relevant Lagrangian autocorrelation functions, and on the requirement that the model be purely dissipative, guaranteeing numerical stability when coupled with the Smagorinsky model. The formulation is tested in forced and decaying isotropic turbulence and in fully developed and transitional channel flow. In homogeneous flows, the results are similar to those of the volume-averaged dynamic model, while in channel flow, the predictions are slightly superior to those of the spatially (planar) averaged dynamic model. The relationship between the model and vortical structures in isotropic turbulence, as well as ejection events in channel flow, is investigated. Computational overhead is kept small (about 10% above the CPU requirements of the spatially averaged dynamic model) by using an approximate scheme to advance the Lagrangian tracking through first-order Euler time integration and linear interpolation in space.

1. Introduction

The dynamic model (Germano *et al.* 1991) is a method for evaluating subgrid-scale (SGS) model coefficients directly from information contained in the resolved turbulent

velocity of a large-eddy simulation (LES). In essence, the model samples turbulent stresses from a band of the smallest resolved scales and then effectively extrapolates this information to the subgrid-scale range. The foundation for the model is the algebraic identity

$$L_{ij} = T_{ij} - \bar{\tau}_{ij}, \tag{1.1}$$

which relates subgrid-scale stresses computed at two different filter widths. The individual terms in the identity are defined as

$$L_{ij} = \widehat{\bar{u}_i\bar{u}_j} - \hat{\bar{u}}_i\hat{\bar{u}}_i, \qquad T_{ij} = \widehat{\bar{u}_i\bar{u}_j} - \hat{\bar{u}}_i\hat{\bar{u}}_j, \quad \text{and} \quad \bar{\tau}_{ij} = \widehat{\bar{u}_i\bar{u}_j} - \widehat{\bar{u}}_i\widehat{\bar{u}}_j. \tag{1.2}$$

In the above expressions, $\bar{()}$ represents filtering at scale Δ, whereas $\hat{()}$ represents filtering at scale 2Δ. $\bar{u}_i(\boldsymbol{x}, t)$ is the resolved turbulent velocity field computed in an LES and τ_{ij} is the corresponding subgrid-scale stress. $\hat{\bar{u}}_i(\boldsymbol{x}, t)$ and T_{ij} are the analogous quantities at scale 2Δ and may be thought of as the velocity and subgrid-scale stress from a hypothetical simulation performed on a coarser mesh. The quantity L_{ij} is the stress formed by turbulent motions of scale intermediate between Δ and 2Δ and is directly computable from the resolved velocity field, $\bar{u}_i$.

The identity is put to use by introducing modelling approximations for τ_{ij} and T_{ij} and then solving for unknown model coefficients. In most applications, the Smagorinsky model is used for (the deviatoric part of) τ_{ij} at scale Δ,

$$\tau_{ij} = -2c_s^2\Delta^2|\bar{S}|\bar{S}_{ij}, \tag{1.3a}$$

and for T_{ij} at scale 2Δ,

$$T_{ij} = -2c_s^2(2\Delta)^2|\hat{\bar{S}}|\hat{\bar{S}}_{ij}. \tag{1.3b}$$

$\bar{S}_{ij}$ and $\hat{\bar{S}}_{ij}$ are the resolved rate-of-strain tensors at scale Δ and 2Δ, respectively. Substitution of these expressions into the Germano identity, (1.1), leads to an over-determined system of five equations for the model coefficient c_s^2. These five equations cannot be satisfied simultaneously, and as a result, it is not possible to satisfy (1.1) exactly within the framework of the Smagorinsky model. The error associated with use of the Smagorinsky model in the Germano identity is defined as

$$e_{ij} = L_{ij} - 2\Delta^2\left[\widehat{c_s^2|\bar{S}|\bar{S}_{ij}} - 4c_s^2|\hat{\bar{S}}|\hat{\bar{S}}_{ij}\right]. \tag{1.4}$$

This error should be minimized, and the various formulations of the dynamic model (beginning with the approaches of Germano *et al.* 1991 and Lilly 1992 – see below) can be interpreted as attempts to minimize the error in different ways. Ghosal *et al.* (1995) observed that c_s^2 appears inside a filtering operation and thus (1.4) is actually a system of integral equations. They used a variational approach to minimize the error in a global least-square sense. This operation leads to a single integral equation for c_s^2 that is solved numerically. Ghosal *et al.* (1995) also showed that simpler expressions for c_s^2 could be derived by including various constraints in the global minimization procedure. For example, if c_s^2 is constrained to have no variation over homogeneous spatial directions, the following algebraic formula arises:

$$c_s^2 = \frac{\langle L_{mn}M_{mn}\rangle}{\langle M_{pq}M_{pq}\rangle}, \tag{1.5}$$

where

$$M_{ij} = 2\Delta^2\left[\widehat{|\bar{S}|\bar{S}_{ij}} - 4|\hat{\bar{S}}|\hat{\bar{S}}_{ij}\right], \tag{1.6}$$

and where $\langle\rangle$ denotes an average over homogeneous directions. In the original work, Germano *et al.* (1991) opted to neglect the spatial variations of c_s^2 and brought it outside the filter operator in (1.4). This operation reduced the integral equations to algebraic ones and the error was minimized locally by requiring that it be orthogonal to the resolved strain-rate tensor. Later Lilly (1992) showed that the equations were better conditioned if the error was made orthogonal to M_{ij}, which corresponds to a least-squares minimization over the independent tensor elements. Lilly's modification leads to an expression identical to (1.5), except for the absence of averaging operators. This expression is often referred to as the local dynamic model.

The local dynamic model was found to predict a highly variable eddy-viscosity field that contained a significant fraction of negative values. The presence of negative eddy viscosity proved to be highly destabilizing in numerical simulations and solutions could not be obtained with the local model. Germano *et al.* (1991) circumvented this problem by averaging the expression for c_s^2 over homogeneous directions. (Although proper justification was lacking at the time, the apparently *ad hoc* averaging operation effectively lead to (1.5), which was derived later by Ghosal *et al.* 1995 using the constrained minimization procedure.) When averaged, the numerator in (1.5) was almost always positive, thus recovering the statistical notion of energy transfer from the resolved to the subgrid scales. Removal of negative eddy viscosity also rectified the stability problem and simulations could be run with the dynamic model. The model was found to give accurate results in a variety of flows where spatial averaging was possible. For example, Germano *et al.* (1991) and Piomelli (1993) obtained accurate results in channel flow by averaging the equations over planes parallel to the walls, and Akselvoll & Moin (1993) obtained similar quality in a backward-facing step flow by averaging over the spanwise direction.

While the averaged formulation effectively stabilizes the model, at least one homogeneous direction is required. This fact precludes the computation of fully inhomogeneous flows. In order to circumvent this limitation, a few attempts have been made to formulate procedures that do not require homogeneous directions. To date, these general formulations have replaced the averaging operation with a constraint in order to stabilize the calculation. Ghosal *et al.* (1995) developed two general models that make use of the global minimization procedure. The first is stabilized by simply imposing the constraint that the model coefficient be non-negative. The second allows for negative eddy viscosity but enforces a budget for the reversed energy transfer through inclusion of a subgrid-scale kinetic energy equation. Piomelli & Liu (1995) have developed a simplified constrained model which is similar to that of Ghosal *et al.* (1995). These general models have been validated in a variety of flows and are applicable to complex-geometry flows under unsteady conditions. While the work of Ghosal *et al.* (1995) and Piomelli & Liu (1995) has provided local methods applicable to fully inhomogeneous flows, some limitations remain. The constraint $c_s^2 \geqslant 0$ is hard to justify on other than heuristic grounds, and the numerical solution of the integral equation in Ghosal's formulation can be expensive (the approximate formulation of Piomelli & Liu 1995 eliminates the additional expense however). The kinetic energy formulation removes the conceptual problem associated with the constraint $c_s^2 \geqslant 0$, but only at the additional expense of two more integral and one transport equation, as well as new heuristic constraints for model coefficients in the kinetic energy equation.

In this paper we develop an alternative general dynamic model that combines some of the best features of the local and averaged formulations. To do this, we enforce the Germano identity in a more average than a local sense. Partial motivation for our approach comes from consideration of the physical processes underlying

the Smagorinsky parameterization. Since the Smagorinsky model is of the eddy-viscosity type, it can only be justified when one considers the ensemble effect of the small-scale motions on much larger scales. It is not apparent that the model should apply on a local, instantaneous level. In support of this line of reasoning, evaluations of the Smagorinsky model from both direct numerical simulation (DNS) (e.g. Clark, Ferziger & Reynolds 1979; McMillan & Ferziger 1979; Meneveau, Lund & Moin 1992) and experimental (Liu, Meneveau & Katz 1994; Meneveau, 1994) data consistently indicate that the model predictions are quite inaccurate on a local level. In fact, poor local agreement has been found even when locally optimized coefficients are used (Lund & Novikov 1992). In light of such findings, it may be more appropriate to enforce the Germano identity in some average sense, instead of insisting that it be obeyed locally. Such a procedure can be viewed as the modern analogue of the statistical approach used by Lilly (1967) to evaluate the Smagorinsky coefficient based on a balance of the *mean* SGS dissipation rate in isotropic turbulence.

In order to incorporate averaging in an inhomogeneous, complex-geometry and unsteady flow, we propose to accumulate the required statistics over fluid-particle trajectories, instead of averaging over directions of statistical homogeneity. Averaging over particle trajectories can be justified by considering the following points. (i) Fluid-particle trajectories are always well defined, Galilean-invariant objects that do not rely on special boundary conditions or assumptions of statistical homogeneity. (ii) Particle trajectories are the natural directions associated with fluid flow and possibly with the turbulent energy cascade. Eddies evolve along particle paths and, as reported by Meneveau & Lund (1994), there is evidence to suggest that the turbulence energy cascade is most apparent when viewed in a Lagrangian frame of reference. Thus it seems natural to postulate that the subgrid-scale model coefficient at a given point $\boldsymbol{x}$ depends on the history of the flow along the trajectory leading to $\boldsymbol{x}$. (iii) As will be shown in §2, averaging increases the validity of the assumption that the same value of c_s^2 applies simultaneously at the two scales Δ and 2Δ.

In §3 we show that averaging along fluid trajectories leads to a pair of relaxation-transport equations that carry the statistics forward in time. We show further that these equations can be solved in an approximate fashion in a numerically efficient way. Several fundamental properties of the Lagrangian model are documented. In §4, the model is applied to a variety of test cases including forced and decaying isotropic turbulence, fully developed channel flow, and transitional channel flow. In each case, the model is shown to produce results equal or superior to those of spatially averaged versions of the dynamic model. At the same time, the numerical solutions to the transport equations increase the computational workload by only about 10% as compared with the spatially averaged approach. A summary and conclusions are given in §5.

We end this section with a further remark on the Smagorinsky model. Although we have chosen to work with this model, our approach is not limited to this parameterization. Several other models have been proposed, some of which have demonstrated advantages over the Smagorinsky model. For example, it is often argued that the local behaviour of SGS stresses is better reproduced by similarity-type models (Bardina, Ferziger & Reynolds 1980; Zang, Street & Koseff 1993; Liu, Meneveau & Katz 1994, 1995). On the other hand, more refined statistical analyses support spectral eddy viscosity (Kraichnan 1976; Leslie & Quarini 1979; Chollet & Lesieur 1981) or hyperviscosity (Morris & Ferziger 1994) models, and also give support for stochastic backscatter models (Leith 1990; Chasnov 1991; Mason & Thomson 1994; Schumann 1995; Carati, Ghosal & Moin 1995). Some of these alternative approaches are not sufficiently dissipative, and they are commonly used in conjunction with a Smagorinsky

term (mixed models). While it is not the purpose of this paper to consider alternative or complementary parameterizations, we remark that the Lagrangian formulation proposed here may be applied to such models in a straightforward manner. As a case in point, Wu & Squires (1995) have recently developed and tested a Lagrangian mixed model.

2. Effects of time averaging on local coefficients at two scales

In this section we use DNS data of isotropic turbulence to study the effects of averaging on the properties of local Smagorinsky coefficients computed at two different scales. In particular, we investigate the effectiveness of time averaging both as a means to reduce high-amplitude spatial variations in the coefficient field, and as a means to limit the occurrence of negative eddy-viscosity values. At the same time, we measure the correlation between coefficients computed at two different scales and quantify the increase in this correlation when either Eulerian or Lagrangian time averaging is used. The results of this study will provide evidence that time averaging enhances the stability of the dynamic model, returns the Smagorinsky model to its proper statistical basis, and improves the accuracy of a key assumption in the dynamic model derivation.

The basic procedure is to filter the DNS data at scale Δ, (a multiple of the mesh spacing), thereby separating it into large-scale and subgrid-scale fields. With the subgrid-scale velocity field known, the subgrid-scale stress and dissipation rate ($\tau_{ij}\bar{S}_{ij}$) are computed exactly. The Smagorinsky coefficient is then computed point-wise by requiring that the modelled SGS dissipation rate equal the exact value at each grid point (Lund, Ghosal & Moin 1993):

$$C_{diss}^{(\Delta)}(\boldsymbol{x},t) = \frac{-\tau_{ij}\bar{S}_{ij}}{\Delta^2(2\bar{S}_{pq}\bar{S}_{pq})^{3/2}}. \tag{2.1a}$$

By filtering at a scale 2Δ, we define an analogous coefficient as

$$C_{diss}^{(2\Delta)}(\boldsymbol{x},t) = \frac{-T_{ij}\tilde{\bar{S}}_{ij}}{(2\Delta)^2(2\tilde{\bar{S}}_{pq}\tilde{\bar{S}}_{pq})^{3/2}}. \tag{2.1b}$$

It should be remarked that this procedure for computing the Smagorinsky coefficient differs from that used in the dynamic model, which only makes use of the stresses formed by the smallest resolved scales. Here we have made use of the exact subgrid-scale stress (which is unknown in LES) to optimize the coefficient.

Using this procedure, we measure $C_{diss}^{(\Delta)}(\boldsymbol{x},t)$ and $C_{diss}^{(2\Delta)}(\boldsymbol{x},t)$ from DNS of forced isotropic turbulence at microscale Reynolds number, $R_\lambda = 95.8$. The data were generated on a 128^3 mesh using the pseudo-spectral code developed by Rogallo (1981). The filters (Δ and 2Δ) were set equal to 4 and 8 mesh units respectively. A physical-space tophat filter was employed at both scales (tests were also performed with Gaussian and cutoff filters). In figure 1(*a*), we show the spatial variability of the coefficient fields, as observed along a line through the database. Large positive and negative excursions can be seen. It is also apparent that the fields at the two scales are only loosely correlated. The correlation coefficient, as calculated over the entire database, is $\rho \approx 0.27$ (the line shown in figure 1 was selected because it has a similar level of correlation). The low correlation is significant since it conflicts with the usual assumption of the local dynamic model, where the coefficient is taken to be the same at the two scales. We will show below that the correlation can be improved

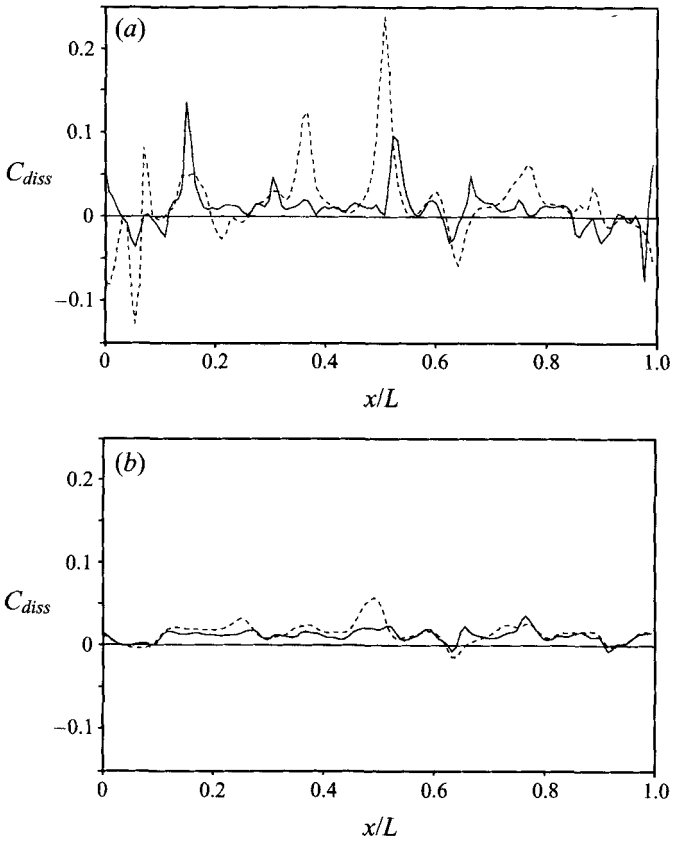

FIGURE 1. Traces of C_{diss} at two filtering scales measured in DNS of isotropic turbulence: (*a*) computed from an instantaneous field, (*b*) computed from an Eulerian average over a time of $3.4\langle\overline{S}_{ij}\overline{S}_{ij}\rangle^{-1/2}$. Solid curve: C^{Δ}_{diss}; dotted curve: $C^{2\Delta}_{diss}$. The traces in (*a*) and (*b*) are for the same line in space. This line was chosen carefully so that the statistics measured along it are very close to those accumulated over the entire field.

significantly by averaging the equations for the coefficients. As an aside, we note that the low correlation between the two coefficients in the local model may justify the use of two model coefficients, as was suggested by Moin (1991).

The effect of temporal averaging was investigated by optimizing the coefficients so that the Eulerian average of the dissipation was predicted correctly. To do this, the simulation was carried forward in time for a period equal to $3.5\langle\overline{S}_{ij}\overline{S}_{ij}\rangle^{-1}$ and a total of 25 fields were saved at nearly equally spaced intermediate times t_n, $n = 1, 2, ...25$ (for more details, see Meneveau & Lund 1994). Coefficients were recomputed with the numerators and denominators in (2.1*a*) and (2.1*b*) averaged in time in an Eulerian fashion. The averaging time scale was varied by including anywhere between 1 and all 25 fields. Figure 1(*b*) shows traces of the two coefficients obtained when the terms in (2.1*a*) and (2.1*b*) are time-averaged over all 25 fields. As can be seen, averaging has decreased the variance, has diminished the frequency of negative coefficients, and has increased the correlation between the two scales.

Figure 2(*a*) shows a plot of the root-mean-square value of the coefficients (both local and time averaged), normalized by their mean value and plotted as a function of the averaging time. At the initial time ($t = 0$), both local and 'averaged' values coincide. The coefficient r.m.s. is seen to drop as the averaging time is increased. It

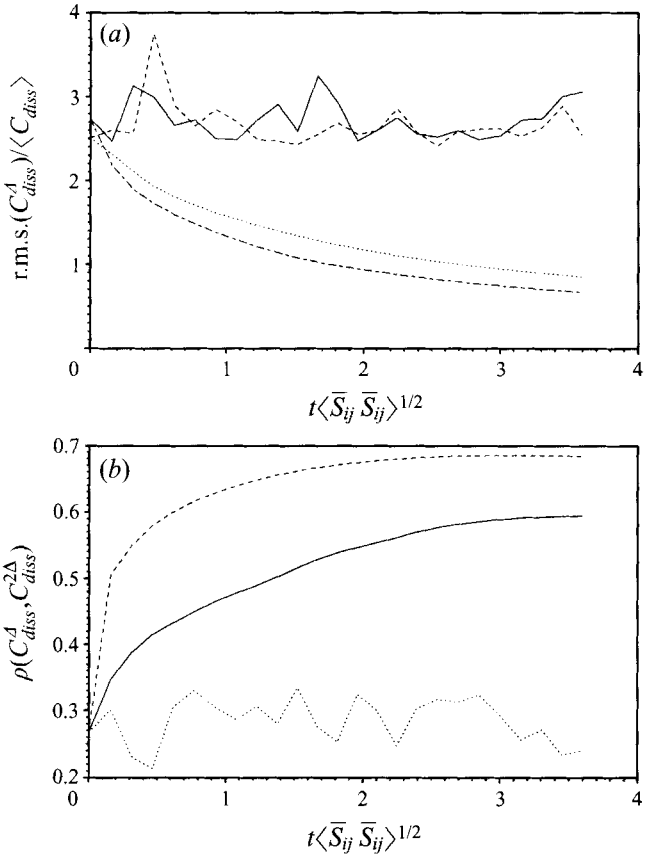

FIGURE 2. (*a*) Root-mean-square values of the dynamic model coefficient, normalized with its mean value, as function of time. The coefficient is defined based on energy dissipation, and is measured from DNS of isotropic turbulence. ——— , Local model, at scale Δ; – – – – , local model, at scale 2Δ; — — — , Eulerian time average, at scale Δ; ····· , Eulerian time average, at scale 2Δ. (*b*) Correlation coefficient between coefficients at two scales Δ and 2Δ, as function of time. ····· , Fully local coefficients; ——— , coefficients obtained after Eulerian time average; – – – – , coefficients obtained after Lagrangian time average, with spatial interpolation.

is also evident that a significant drop in r.m.s. is achieved by averaging over a fairly short interval. In particular, an averaging interval of roughly two grid-scale turnover times (as measured by $\langle \overline{S}_{ij}\overline{S}_{ij}\rangle^{-1}$) is sufficient to produce more than 60% of the asymptotic r.m.s. drop. Averaging also reduces the frequency of negative coefficient values. Figure 2(*b*) shows the correlation between the coefficients at the two scales. The lower curve, corresponding to the instantaneous coefficients, fluctuates around $\rho \sim 0.27$. The correlation between the averaged coefficient fields, however, rises to a value close to 0.6. Again much of the change takes place in the order of two grid-scale turnover times. Similar increase in correlation was observed when the tophat filter was replaced by a Gaussian. (A rise with respect to its initial value was also observed when using the cutoff filter, but at very low levels – from $\rho \sim 10^{-3}$ to $\rho \sim 0.03$.)

The dashed line in figure 2(*b*) shows the correlation when time averaging is performed along fluid-particle trajectories (Lagrangian). The method employed to follow fluid trajectories uses bilinear interpolation between grid points, and is the same as described in Meneveau & Lund (1994). The higher correlation in this case can be

attributed to even lower r.m.s., due to the additional smoothing that occurs from spatial interpolations in the Lagrangian tracking scheme.

The results presented here suggest that optimizing the Smagorinsky coefficient from time averaged rather than instantaneous fields has several benefits. In particular, the frequency of occurrence of negative values is reduced and the correlation between coefficients computed at two scales is increased. These factors are significant since a reduction in negative values enhances stability (we will later propose an averaging scheme that eliminates negative values altogether), while an increased correlation between the two scales increases the validity of an assumption in the dynamic model derivation. On a more physical level, time averaging adds a statistical element which we feel should be present in the Smagorinsky parameterization (for experimental evidence supporting a statistical instead of a purely local interpretation of this model, see Meneveau 1994). It is also important to note that averaging over a few small-scale turn-over times is sufficient to produce these benefits while still allowing for considerable spatial variation in the coefficient field (figure 1*b*). This issue will be discussed in more detail in §3.5 where the relationship between flow structures and the coefficient field is studied.

As a final note, we should mention that the Lagrangian model will reduce temporal as well as spatial fluctuations. Once again, we see this as more of a strength than a weakness since meaningful low-frequency variations are accounted for directly while high-frequency fluctuations are represented only in an average sense.

3. The Lagrangian dynamic model

3.1. *Formulation*

The Lagrangian model is derived by minimizing the error incurred by inserting the Smagorinsky model in the Germano identity along fluid-particle trajectories. The derivation is most natural in a Lagrangian frame of reference and we start by considering a fluid particle located at position $\boldsymbol{x}$ at time t. Its trajectory for earlier times $t' < t$ is given by

$$\boldsymbol{z}(t') = \boldsymbol{x} - \int_{t'}^{t} \bar{\boldsymbol{u}}[\boldsymbol{z}(t''), t'']\,\mathrm{d}t''. \tag{3.1}$$

In terms of the Lagrangian description the error to be minimized, (1.4), is

$$e_{ij}(\boldsymbol{z}, t') = L_{ij}(\boldsymbol{z}, t') - c_s^2(\boldsymbol{x}, t) M_{ij}(\boldsymbol{z}, t'), \tag{3.2}$$

where M_{ij} is defined in (1.6). Note that we have removed $c_s^2(\boldsymbol{x}, t)$ from the filter operation, by assuming that it does not vary strongly in space over the scale of the test filter. *A posteriori* justification for this assumption is based on the fact that $c_s^2(\boldsymbol{x}, t)$ is determined from averaged equations. In §3.6, we use isotropic turbulence to study the error associated with this assumption.

The model coefficient to be used at time t and position $\boldsymbol{x}$ ($c_s^2(\boldsymbol{x}, t)$) is determined by minimizing the error over the trajectory of the fluid particle. In other words, we employ previous information along the pathline in order to determine the current value of the coefficient. The total error which is to be minimized is defined as the pathline accumulation of the local error squared,

$$E = \int_{-\infty}^{t} e_{ij}(\boldsymbol{z}(t'), t')\, e_{ij}(\boldsymbol{z}(t'), t')\, W(t - t')\, \mathrm{d}t' \tag{3.3}$$

The weighting function $W(t - t')$ is introduced here in order to control the relative

importance of events near time t with those of earlier times. As described below, we shall weight the error at time t most strongly and assign a decreasing weight to earlier times. The total error is then minimized with respect to c_s^2 by enforcing

$$\frac{\partial E}{\partial c_s^2} = \int_{-\infty}^{t} 2e_{ij} \frac{\partial e_{ij}}{\partial c_s^2} \, W(t-t') \, \mathrm{d}t' = 0. \tag{3.4}$$

Making use of (3.2) and solving for c_s^2, one obtains

$$c_s^2(\boldsymbol{x},t) = \frac{\mathscr{I}_{LM}}{\mathscr{I}_{MM}}, \tag{3.5}$$

where

$$\mathscr{I}_{LM}(\boldsymbol{x},t) = \int_{-\infty}^{t} L_{ij} M_{ij}(\boldsymbol{z}(t'),t') \, W(t-t') \, \mathrm{d}t', \tag{3.6}$$

$$\mathscr{I}_{MM}(\boldsymbol{x},t) = \int_{-\infty}^{t} M_{ij} M_{ij}(\boldsymbol{z}(t'),t') \, W(t-t') \, \mathrm{d}t'. \tag{3.7}$$

The function $W(t-t')$ is a free parameter, essentially defining the extent backward along the pathline over which we choose to minimize the error. Although several appropriate weighting functions are possible, an exponential weighting of the form $W(t-t') = T^{-1}\mathrm{e}^{-(t-t')/T}$ has the distinct practical advantage that the integrals $\mathscr{I}_{LM}$ and $\mathscr{I}_{MM}$ are solutions to the following relaxation-transport equations:

$$\frac{\mathrm{D}\mathscr{I}_{LM}}{\mathrm{D}t} \equiv \frac{\partial \mathscr{I}_{LM}}{\partial t} + \bar{\boldsymbol{u}} \cdot \nabla \mathscr{I}_{LM} = \frac{1}{T}\left(L_{ij}M_{ij} - \mathscr{I}_{LM}\right), \tag{3.8}$$

$$\frac{\mathrm{D}\mathscr{I}_{MM}}{\mathrm{D}t} \equiv \frac{\partial \mathscr{I}_{MM}}{\partial t} + \bar{\boldsymbol{u}} \cdot \nabla \mathscr{I}_{MM} = \frac{1}{T}\left(M_{ij}M_{ij} - \mathscr{I}_{MM}\right). \tag{3.9}$$

In the context of LES, solving such transport equations is much more natural than having to perform integrals backwards in time according to (3.6) and (3.7). Figure 3 illustrates the basic idea of averaging over pathlines with an exponentially decreasing memory. This picture should be contrasted with that of conventional schemes where global spatial averaging completely removes information about the flow structure, and the turbulence development history is completely ignored. Eulerian time averaging suffers from similar deficiencies, since the advection of structures is ignored. Also noteworthy is the partial resemblance with the $k-\epsilon$ model; the Lagrangian dynamic eddy viscosity also involves the ratio of two variables, each of which is the (history-dependent) solution of a transport equation.

3.2. *Relaxation time scale*

The time scale T controls the memory length of the Lagrangian averaging, and several choices can be made. In §2 we found that averaging on the time scale of the smallest resolved turbulent motions was sufficient to eliminate unwanted noise and improve the correlation between coefficients at two different scales. In light of these findings, it seems appropriate to base the averaging interval on a characteristic time for motions near the grid scale. Some possible choices are the following: (*a*) $T \sim |\bar{S}|^{-1}$, (*b*) $T \sim |\bar{S}|^{-1}$, (*c*) $T \sim \Delta(M_{ij}M_{ij})^{-1/4}$, (*d*) $T \sim \Delta(L_{ij}M_{ij})^{-1/4}$, (*e*) $T \sim \Delta\mathscr{I}_{MM}^{-1/4}$, (*f*) $T \sim \Delta\mathscr{I}_{LM}^{-1/4}$, and (*g*) $T \sim \Delta[\mathscr{I}_{LM}\mathscr{I}_{MM}]^{-1/8}$. In fully developed turbulence, all of these time scales are of the same order of magnitude. The first four choices are based on local values, which makes T is a strongly fluctuating variable. Options (*e–g*) are based on the smoother Lagrangian averages, which is preferable.

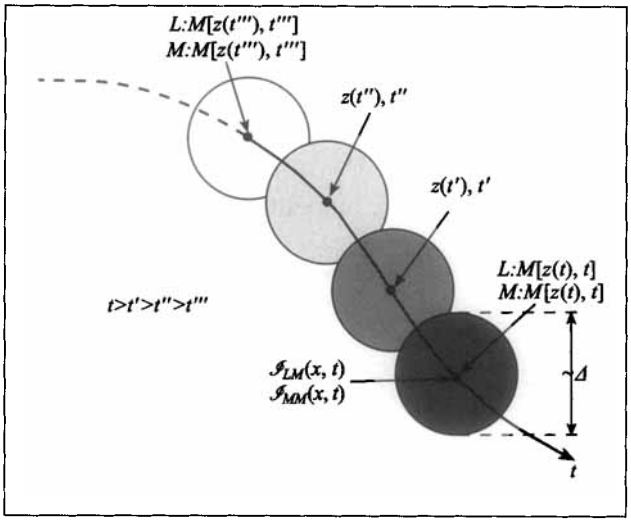

FIGURE 3. Sketch of fluid trajectory of the resolved LES velocity field. The error associated with the Germano identity is weighted with an exponentially decreasing function (indicated as different grey levels), backwards in time, to yield a current value for the model coefficient at point x and time t.

We have chosen to use option (g), which has the following useful properties. Since it depends on both $\mathcal{I}_{MM}$ and $\mathcal{I}_{LM}$, the memory time is reduced in regions of high straining (where $\boldsymbol{M}^2$ is large), as well as in regions of large nonlinear energy transfer (where $L_{ij}M_{ij}$ is large). Furthermore, if $L_{ij}M_{ij} \leqslant 0$ for a persistent time along the pathline, then $\mathcal{I}_{LM}$ approaches zero. T evaluated according to (g) then tends to ∞, i.e. the memory time increases. In other words, the current values are weighted less strongly relative to the past ones, if they are of the backscattering type. This is useful in the implementation with the Smagorinsky model where we wish to restrict the Smagorinsky expression for the modelling of energy dissipation only. The expressions for c_s are weighted much less heavily when $L_{ij}M_{ij} \leqslant 0$ in a persistent fashion, i.e. we opt for 'learning' as little as possible about the coefficient from the resolved field when it would predict backscatter.

Equation (3.8) can now be written as

$$\frac{\mathrm{D}\mathcal{I}_{LM}}{\mathrm{D}t} = \frac{1}{\theta\Delta}(\mathcal{I}_{LM}\mathcal{I}_{MM})^{1/8}\left(L_{ij}M_{ij} - \mathcal{I}_{LM}\right), \tag{3.10}$$

where θ is a dimensionless coefficient of order unity. If $\mathcal{I}_{LM}$ reaches zero, its rate of change is zero as well. Therefore, $\mathcal{I}_{LM}$ cannot become negative, and the resulting dynamic model will not suffer from numerical instability due to negative eddy viscosities. We point out, however, that if $L_{ij}M_{ij} \leqslant 0$, the approach of $\mathcal{I}_{LM}$ to zero is not exponential, but of the power-law type (as $(t_0 - t)^{8/7}$). This means that after the (finite) time t_0 at which $\mathcal{I}_{LM} = 0$, the solution becomes complex. Thus, in practice, the solution must still be 'clipped' to zero during such times. This type of clipping is much less drastic than previous approaches since it is only required occasionally, and because c_s^2 approaches zero with zero slope.

A judicious choice for the dimensionless coefficient θ must now be made. Intuitively, we must average over a few 'events' of the variable $L_{ij}M_{ij}$ or $M_{ij}M_{ij}$ along the pathline. The average duration of such events is expected to be of the order of $\Delta(\langle L_{ij}M_{ij}\rangle\langle M_{ij}M_{ij}\rangle)^{-1/8}$, but in order to quantify this assertion, we analyze results

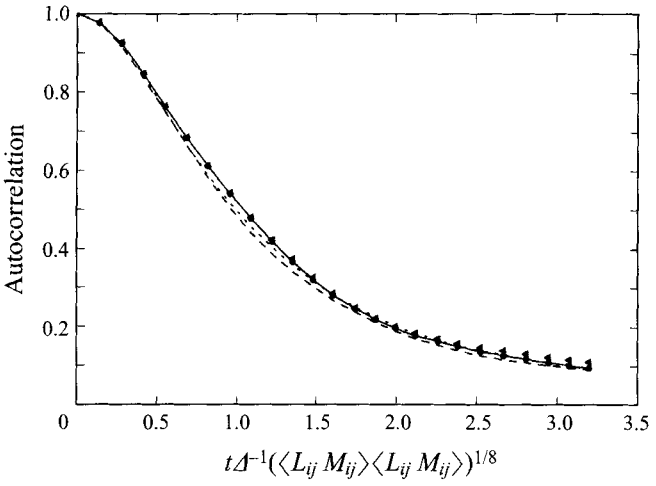

FIGURE 4. Lagrangian and Eulerian autocorrelation functions calculated from a filtered DNS of forced isotropic turbulence. —●—, Lagrangian autocorrelations of $L_{ij}M_{ij}$; ▲, Lagrangian autocorrelations of $M_{ij}M_{ij}$; – – – –, Eulerian temporal autocorrelations of $L_{ij}M_{ij}$; ·····, Eulerian temporal autocorrelations of $M_{ij}M_{ij}$.

from DNS of forced isotropic turbulence. The goal is to compute the Lagrangian autocorrelation function of the scalar variables $L_{ij}M_{ij}$ and $M_{ij}M_{ij}$. We employ the same tracking method as described in §2. For comparison, we also compute their Eulerian fixed-point two-time autocorrelation functions. The Lagrangian tracking was done in the sequence of DNS velocity fields described in §2. Each field was filtered with a Fourier cutoff filter at a scale corresponding to 4 mesh spacings. Lagrangian and Eulerian autocorrelations were then computed for quantities derived from the filtered velocity fields.

Figure 4 shows the computed autocorrelations. As expected, the Lagrangian autocorrelations decay at a slower rate than the Eulerian ones, but the difference is small due to the fact that the mean velocity of this flow is zero. Also, the decay of the LM and MM terms is quite similar. After a time-delay $\sim \frac{3}{2}\Delta[\langle L_{ij}M_{ij}\rangle\langle M_{ij}M_{ij}\rangle]^{-1/8}$, the autocorrelation has already fallen below the $1/e$ point. This suggests that averaging over Lagrangian time spans equal to this interval is sufficient to significantly smooth instantaneous fluctuations. In summary, during the present work we choose

$$T = \theta\ \Delta\ (\mathscr{I}_{LM}\mathscr{I}_{MM})^{-1/8}; \qquad \theta = 1.5 \tag{3.11}$$

as the time scale characterizing the exponential memory with which the Germano identity is enforced. An analysis of the sensitivity of LES to this choice of θ will be performed when applying the model to a non-homogeneous flow (channel flow in §4.3).

3.3. *Numerical method*

In principle, the implementation of the Lagrangian dynamic model requires the solution of two additional transport equations ((3.8) and (3.9)) during the LES. This undoubtedly increases the computational cost associated with the subgrid modelling. However, the considerable flexibility of choice of the averaging domain suggests that high numerical accuracy in solving (3.8) and (3.9) may be unnecessary. Therefore, we

use a particularly simple formulation based on discretizing (3.8) in time as follows:

$$\frac{\mathscr{I}_{LM}^{n+1}(\boldsymbol{x}) - \mathscr{I}_{LM}^{n}(\boldsymbol{x} - \overline{\boldsymbol{u}}^{n}\Delta t)}{\Delta t} = \frac{1}{T^{n}}\left([L_{ij}M_{ij}]^{n+1}(\boldsymbol{x}) - \mathscr{I}_{LM}^{n+1}(\boldsymbol{x})\right). \tag{3.12}$$

Equation (3.9) is dealt with in a similar manner. Positions $\boldsymbol{x}$ are coincident with grid points of the simulation. The value of $\mathscr{I}_{LM}^{n}$ at the previous time step and at the upstream location $\boldsymbol{x} - \overline{\boldsymbol{u}}^{n}\Delta t$ can be obtained by multilinear interpolation. Finally, the new values at the grid points are solved for. The result is a weighted sum of the interpolated prior value and the current source term at the grid point:

$$\mathscr{I}_{LM}^{n+1}(\boldsymbol{x}) = H\left\{\epsilon\,[L_{ij}M_{ij}]^{n+1}(\boldsymbol{x}) + (1-\epsilon)\mathscr{I}_{LM}^{n}(\boldsymbol{x} - \overline{\boldsymbol{u}}^{n}\Delta t)\right\} \tag{3.13}$$

and

$$\mathscr{I}_{MM}^{n+1}(\boldsymbol{x}) = \epsilon\,[M_{ij}M_{ij}]^{n+1}(\boldsymbol{x}) + (1-\epsilon)\mathscr{I}_{MM}^{n}(\boldsymbol{x} - \overline{\boldsymbol{u}}^{n}\Delta t), \tag{3.14}$$

where

$$\epsilon \equiv \frac{\Delta t/T^{n}}{1 + \Delta t/T^{n}}, \quad \text{and} \quad T^{n} = 1.5\,\Delta\,(\mathscr{I}_{LM}^{n}\mathscr{I}_{MM}^{n})^{-1/8}, \tag{3.15}$$

and where $H\{x\}$ is the ramp function ($H\{x\} = x$ if $x \geqslant 0$, and zero otherwise). The ramp function is introduced to clip the solution away from complex values.

Finally, we point out that the approximate spatial interpolation between grid points inevitably introduces some numerical diffusion into (3.8) and (3.9). Physically, such diffusion acts to smooth the $\mathscr{I}_{LM}$ and $\mathscr{I}_{MM}$ fields, and can be interpreted as an additional local spatial average. Although we observed no adverse effects of numerical diffusion, it could be reduced if necessary by the use of higher-order interpolation operators (although only at additional numerical cost).

3.4. *Statistical features of the model*

As a next step, the model is implemented in LES of forced isotropic turbulence on a 32^3 grid, using a variant of the Rogallo (1981) code. Forcing is achieved by holding the Fourier amplitudes fixed within the sphere $k < 2$. Test filtering is achieved through a Fourier cutoff at twice the grid scale.

The velocity field is initialized in the usual manner by superposing Fourier modes with a prescribed spectrum but random phases, and projection onto the divergence-free space. Additionally, the initial condition for the fields $\mathscr{I}_{LM}$ and $\mathscr{I}_{MM}$ must be prescribed. For initializations corresponding to turbulent flows, we propose to set

$$\mathscr{I}_{MM}(\boldsymbol{x},0) = M_{ij}M_{ij}(\boldsymbol{x},0), \quad \mathscr{I}_{LM}(\boldsymbol{x},0) = c_s^2(0)\,M_{ij}M_{ij}(\boldsymbol{x},0), \tag{3.16}$$

where $c_s^2(0) = 0.16^2 = 0.0256$ is the traditional value of the Smagorinsky constant. Thus at the initial time, the model involves a position-independent, prescribed coefficient. For initializations corresponding to laminar flows, we propose to set $c_s = 0$ in the above expressions.

When the LES of forced isotropic turbulence is started, fluctuations of the Lagrangian dynamic coefficient c_s quickly build as different values of $L_{ij}M_{ij}$ begin to affect the averages. Once a statistical steady state has been reached, these fluctuations are characterized by the probability density function of the coefficient shown by solid circles in figure 5. Notice the small spike at $c_s = 0$, arising from the regions in which c_s is clipped at zero, away from complex values (on about 5% of the points in this case). Initial transients leading to such a steady-state distribution are relatively short. This can be appreciated by observing the time development of the p.d.f.s when the 'wrong' initial condition is employed for $c_s(0)$. In one case, we start with $c_s^2(0) = 0.005$, and in

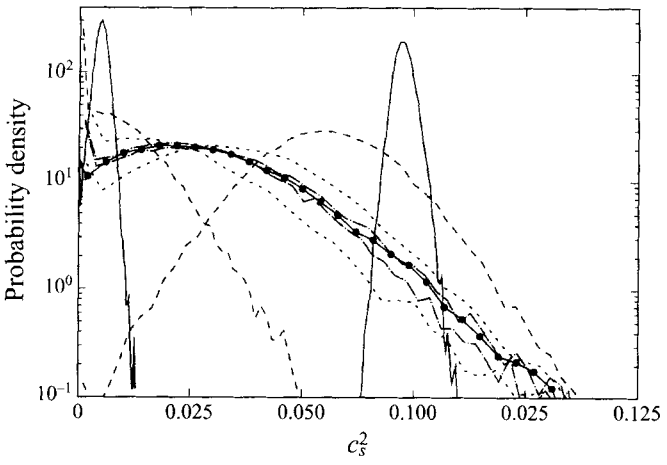

FIGURE 5. Probability density functions of the coefficient c_s^2, computed from the Lagrangian dynamic model in a pseudo-spectral LES of forced isotropic turbulence at $Re = \infty$, on a 32^3 mesh. The circles represent the asymptotic p.d.f. long after initial transients have passed (obtained here at $t = 12\langle T\rangle$, where $\langle T\rangle = 1.5\Delta(\langle L_{ij}M_{ij}\rangle\langle L_{ij}M_{ij}\rangle)^{-1/8}$). Evolving p.d.f.s on both sides illustrate how delta function p.d.f.s with the wrong initial conditions quickly reach the asymptotic statistics. Curves that peak to the left of the asymptotic curve correspond to $c_s^2(0) = 0.005$; those peaking to the right evolve starting from $c_s^2 = 0.075$. ——— , 1 time step; – – – – , $t = 0.2\langle T\rangle$; ····· , $t = 0.9\langle T\rangle$; —·— , $t = 1.9\langle T\rangle$. For reference, the time scale associated with the resolved strain rate is $\langle \bar{S}_{ij}\bar{S}_{ij}\rangle^{-1/2} = 0.5\langle T\rangle$.

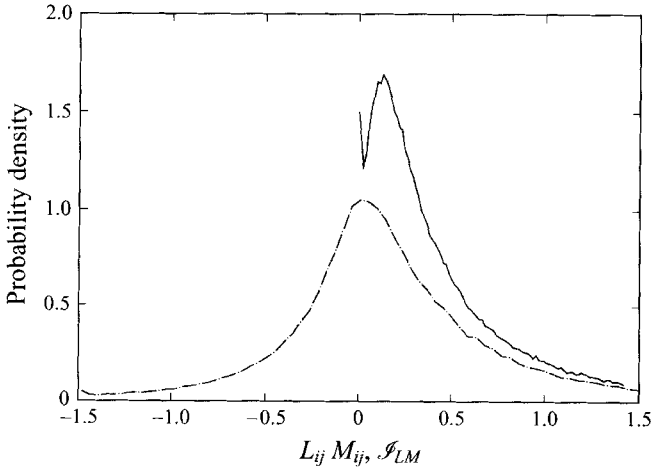

FIGURE 6. Probability density functions of numerators: —·— : evaluated locally $(L_{ij}M_{ij})$; ——— , after Lagrangian averaging $(\mathcal{I}_{LM})$. These distributions are calculated from a 32^3-node, pseudo-spectral LES of forced isotropic turbulence that uses the Lagrangian dynamic Smagorinsky model. To increase the sample, p.d.f.s are accumulated over several independent fields. The spike at the origin represents a δ-function that integrates to 0.05.

another case with $c_s^2(0) = 0.075$. In both cases the asymptotic distribution is reached after times of the order of $2\langle T\rangle$ where T is the time scale defined by (3.11). We conclude that the proposed method of initialization is acceptable since the simulation 'forgets' the initial state after only few grid-scale turnover times. This is comparable to the time it takes the simulation to build up realistic phases in the resolved velocity field, starting from the random-phase initial condition.

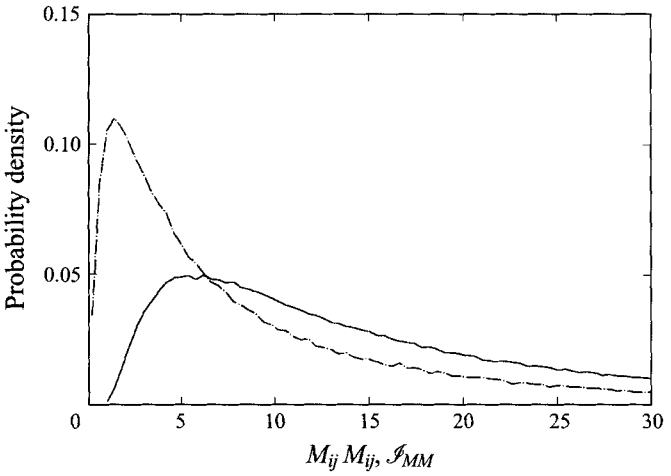

FIGURE 7. Probability density functions of denominators: —·—, evaluated locally ($M_{ij}M_{ij}$); ———, after Lagrangian averaging ($\mathscr{J}_{MM}$). Details as in figure 6.

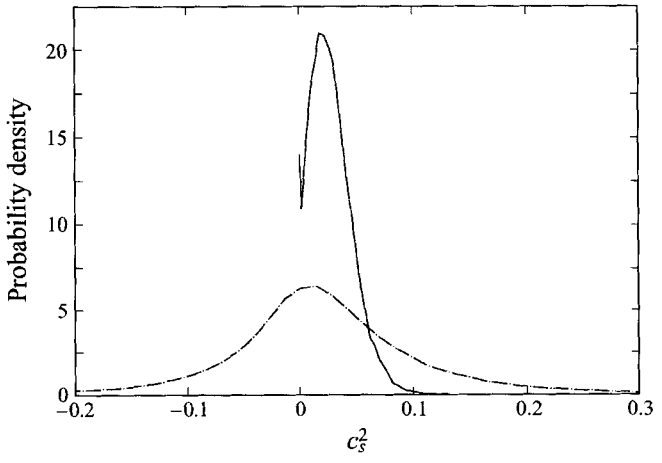

FIGURE 8. Probability density functions of model coefficients taken from a 32^3 Lagrangian dynamic model LES of forced isotropic turbulence: —·—, coefficient evaluated locally; ———, coefficient from the Lagrangian model. The spike at the origin represents a δ-function that integrates to 0.05.

To further document the effect of the Lagrangian averaging, we compute the probability density functions of $\mathscr{J}_{LM}$ and $\mathscr{J}_{MM}$ and compare them with those of the local values $L_{ij}M_{ij}$ and $M_{ij}M_{ij}$. Figures 6 and 7 show these results. As expected, the distributions become narrower after the Lagrangian averaging. By construction, there are no negative values of $\mathscr{J}_{LM}$. In terms of denominators, the averaging is seen to virtually eliminate values near zero. The p.d.f. of $\mathscr{J}_{MM}$ approaches the origin with negligible slope while the probability of the local value of $M_{ij}M_{ij}$ being close to zero is considerable. In figure 8, we show the measured p.d.f. of the coefficient c_s^2 itself. As can be seen, the variance of the coefficient in the local formulation is greatly reduced by the Lagrangian averaging. Also, no negative values exist although a finite number of points ($\sim 5\%$) exhibit $c_s^2 = 0$ as indicated by the small spike at the origin.

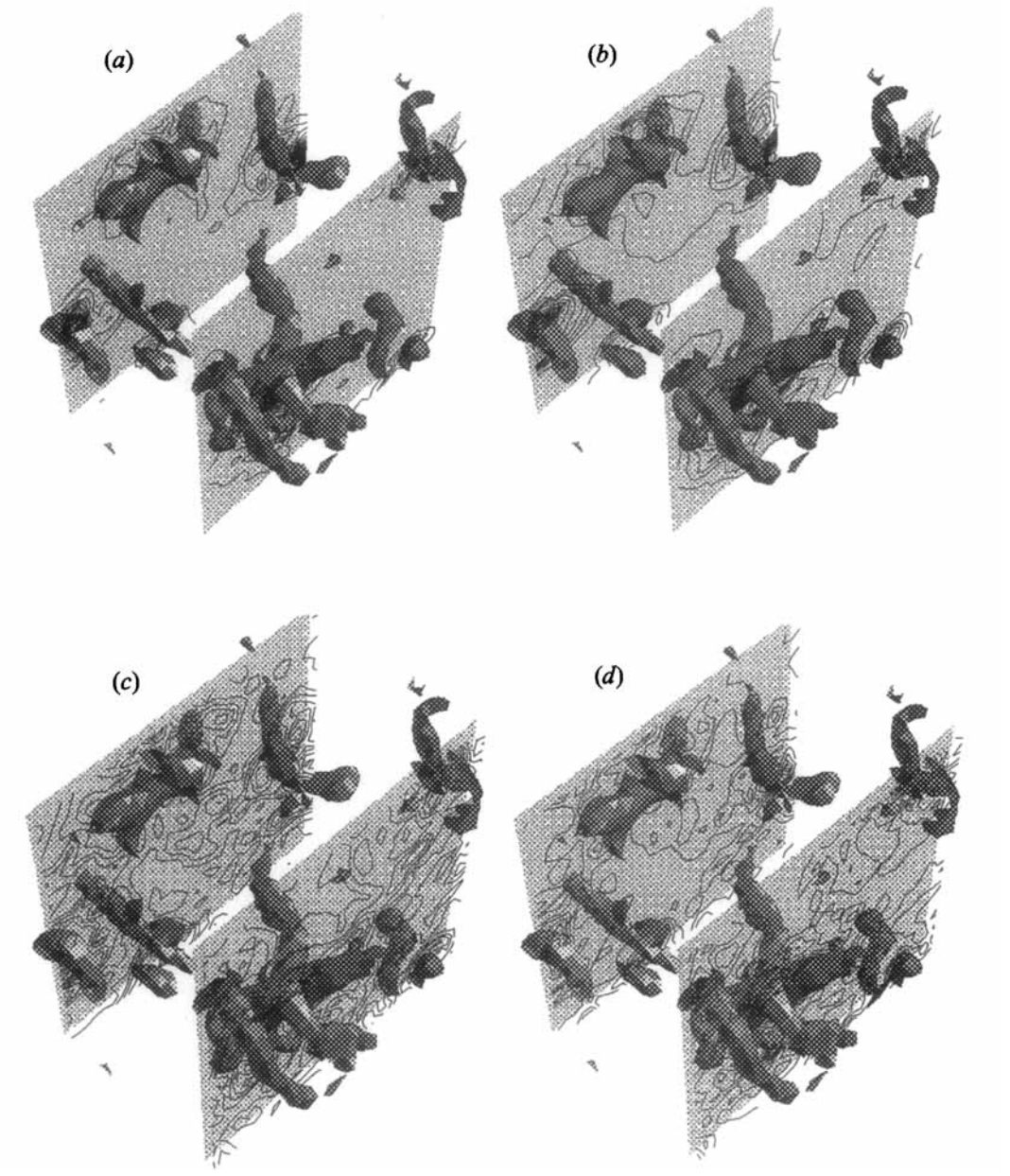

FIGURE 9. Visualization of high-magnitude vorticity regions in LES of isotropic forced turbulence at $Re = \infty$. Surfaces correspond to points at which $|\overline{\omega}| = 2.4\langle\overline{\omega}^2\rangle^{1/2}$. On planes, contours of different variables are shown: (*a*) $\mathscr{I}_{LM}$, (*b*) $\mathscr{I}_{MM}$, (*c*) $|\overline{S}|$ (proportional to eddy viscosity with volume-averaged coefficient) and (*d*) $(\mathscr{I}_{LM}/\mathscr{I}_{MM})\,|\overline{S}|$ (proportional to eddy viscosity computed from the Lagrangian dynamic model).

3.5. *Relationship to vortical flow structures*

The goal of this section is to make qualitative observations pertaining to possible relations between the terms $\mathscr{I}_{LM}$, $\mathscr{I}_{MM}$, and discernible flow structures that may appear in the resolved velocity field during LES.

First, we report the existence of tubular structures that characterize regions in which

the resolved vorticity vector has high magnitude, in our 32^3 LES. Figure 9 shows iso-surfaces of vorticity magnitude (at a threshold of $|\omega|_{th} = 2.4\langle\omega^2\rangle^{1/2}$). Clearly, 'fat worms' exist in the solution. The existence of tubular vortical structures in LES has also been observed recently by Briscolini & Santangelo (1994), using a different subgrid model. One interesting question to be answered is whether the prediction of such 'fat worms' by LES is realistic. We recall that DNS predicts worms with very small diameters of about four Kolmogorov scales (Jimenez *et al.* 1993). Surely they cannot be captured by an LES at $Re = \infty$. The relevant question is whether a field generated by DNS and then low-pass filtered at inertial-range scales comparable to the LES grid size exhibits 'fat worms' that are comparable to those predicted by LES. We have performed such an operation based on the 128^3 forced DNS described earlier and have visualized regions of high vorticity magnitude. We indeed observed 'fat worms' that were of similar appearance than those of the LES (see also figure 17 of Vincent & Meneguzzi 1991). It must be recognized that the 'high-vorticity' regions in the filtered DNS correspond to much lower vorticity magnitudes than those of the unfiltered fields. This is the reason why these 'fat worms' are not visible when analysing the unfiltered DNS fields. In summary, we observe elongated vortical regions in LES and believe that their existence is a realistic prediction by the simulation since they also exist in low-pass-filtered DNS fields.

The next issue to be addressed is whether the Lagrange-averaged quantities that enter our dynamic model bear any relationship to such local structures. Figure 9(*a*) shows contour plots of $\mathscr{I}_{LM}$ on two planes of the computational cube, selected to cut some of the most visible vortical structures. The field is chosen at some time long after the simulation has reached statistical steady state. Figure 9(*b*) shows a similar graph for $\mathscr{I}_{MM}$. Generally, it is apparent that the contours of both $\mathscr{I}_{LM}$ and $\mathscr{I}_{MM}$ are somewhat 'correlated' with the presence of worms. The contours peak in the neighbourhood of the worms while not much activity is seen in regions that are far removed from the structures. Upon closer examination, we observe that the peaks in $\mathscr{I}_{LM}$ and $\mathscr{I}_{MM}$ are most often located near the cores of the worms but not inside them. Many times the maximum values occur between two closely spaced worms. These are expected to be regions of large straining and turbulence generation. Also, correlation is seen between fields $\mathscr{I}_{LM}$ and $\mathscr{I}_{MM}$, which is instrumental in decreasing the variance of the predicted model coefficient.

Clearly, a detailed understanding of the relationship between the coefficient c_s^2 and local flow structures, and of their dynamical interplay and relevance, is still elusive. Nevertheless, we have shown that the Lagrangian averaging preserves some spatial locality in the model. Spatially localized events in the numerators and denominators used to compute the model coefficient have some relationship to local flow structures. The volume-averaged dynamic model would have generated a position-independent coefficient that is oblivious to local flow structures. To observe the effect on the predicted eddy viscosity, figures 9(*c*) and 9(*d*) show contour plots of the strain-rate magnitude $|\overline{S}|$ and of the expression $(\mathscr{I}_{LM}/\mathscr{I}_{MM})|\overline{S}|$. The former is proportional to the eddy viscosity predicted with a volume-averaged coefficient while the latter is proportional to the eddy viscosity predicted by the Lagrangian dynamic model. Both show peaks surrounding the worms, but the precise location of these peaks differs. Also, the Lagrangian dynamic eddy viscosity appears to be more concentrated near the structures while being lower and fluctuating less in the regions far away from the structures.

3.6. *Error in extracting c_s^2 from the filtering operation*

In §3.1 it was assumed in advance that, by virtue of the averaging process, c_s^2 should vary negligibly over the scale of the test filter. This assumption allowed c_s^2 to be extracted from the filter operation, thereby reducing the problem from an integral equation to an algebraic one. In this section we will (partially) justify this approximation *a posteriori* by quantifying the error introduced by neglecting the spatial variation of c_s^2 in the test filtering operation.

The approximation made in (3.2) amounts to replacing $\widehat{c_s^2|\overline{S}|\overline{S}_{ij}}$ with $c_s^2\widehat{|\overline{S}|\overline{S}_{ij}}$ in (1.4). Although this is a poor approximation if (3.2) were solved locally, the error can be reduced to acceptable levels if c_s^2 is determined by some averaged version of (1.1). Most previous versions of the dynamic model have employed spatial averaging to reduce (or eliminate) the error in removing c_s^2 from the test filter operation (as noted before, an exception is in the work of Ghosal *et al.* 1995 where the spatial variation of c_s^2 is taken into account through the solution of an integral equation). In this work we rely on the Lagrangian time average to smooth the spatial variations of the model coefficient so that c_s^2 is approximately constant over the scale of the test filter (two mesh cells).

The efficacy of our approach is evaluated here by comparing the error when Lagrangian averaging is performed and when (1.4) is solved directly (i.e. with no averaging). We define the error, η, as the r.m.s. of the difference between $A_{ij} \equiv \widehat{c_s^2|\overline{S}|\overline{S}_{ij}}$ and $B_{ij} \equiv c_s^2\widehat{|\overline{S}|\overline{S}_{ij}}$. Errors are scaled with the r.m.s. of A_{ij} of the unaveraged (local) case. Thus

$$\eta = \frac{\langle (A_{ij} - B_{ij})(A_{ij} - B_{ij}) \rangle^{1/2}}{\left(\langle A_{lm} A_{lm} \rangle - \langle A_{lm} \rangle \langle A_{lm} \rangle \right)_{\text{local}}^{1/2}}, \tag{3.17}$$

where $\langle\rangle$ denotes an average over the volume. η is evaluated in 128^3 and 32^3 LES of forced isotropic turbulence (to be described in more detail in §4.1). The error was found to be $\eta = 1.3$ for the local case (no averaging), and only $\eta = 0.18$ when the coefficient is obtained after Lagrangian averaging. Thus, Lagrangian averaging significantly reduces the magnitude of the error. Of course it also reduces the r.m.s. of A_{ij} and B_{ij}, so that the relative error (defined by scaling with the r.m.s. of A_{ij} obtained from Lagrangian averaging) decreases less dramatically. But, one still obtains smaller values than for the local case ($\eta = 0.51$ for the 128^3 simulation, and $\eta = 0.33$ for the 32^3 simulation).

In the case of isotropic turbulence, the error in removing the coefficient from the test filter operation could be reduced further by increasing the Lagrangian average time scale (increasing the parameter θ in (3.11)). Increasing the time scale, however, limits the ability of the model to respond to local variations in space and time, and in fact was found to lead to a slight degradation in the LES results for turbulent channel flow (to be discussed in §4.3). Thus a compromise must be made between mathematical consistency and the ability of the model to reflect the local state of the flow. We believe that $\theta = 1.5$ is a good compromise and the resulting error is acceptable for typical LES purposes. The test cases presented in §4 support this conjecture and it appears that an error of the size observed here does not have an adverse effect on the LES results.

It is important to note that the forgoing analysis is for a homogeneous flow where space and time averages converge as the sample becomes large. Thus the Lagrangian average is certain to reduce the spatial variability of c_s^2. Inhomogeneous flows will

not necessarily behave in the same manner, however, and it is possible that stronger fluctuations at the scale of the test filter may be present, even after long Lagrangian averaging. For applications in which this issue is thought to be critical, we note that the errors associated with extracting c_s^2 from the test filter operation can be reduced to an arbitrary level if our model is reformulated in terms of the approximate localization model of Piomelli & Liu (1995). This would involve a straightforward redefinition of the numerator and denominators to be Lagrangian averaged.

4. Applications

In this section, we report applications of the Lagrangian dynamic model to several test cases. We consider forced and decaying isotropic turbulence, as well as transitional and fully developed channel flow. While these flows could have been treated with the spatially averaged dynamic model, our purpose in choosing these simple flows is to test the model in a controlled setting where other (less general) dynamic model formulations have produced good results. We will also compare a few of our results with spatially averaged dynamic model predictions in order to highlight some important differences. Tests such as these are a necessary first step before applications to unsteady and complex-geometry flows are attempted where many other effects such as numerics, etc. may influence the results and obscure the role of the subgrid model. A variant of the Lagrangian model has also been tested with success by Wu & Squires (1995) in LES of a three-dimensional boundary layer and Wang & Squires (1996) in particle-laden channel flow.

4.1. *Forced isotropic turbulence*

LES of forced isotropic turbulence is performed on both 32^3 and 128^3 grids, using the code already described in §3.4. The simulation is run for 15000 and 6000 time steps on the 32^3 and 128^3 grids, respectively.

Figures 10(*a*) and 10(*b*) show the resulting radial energy spectra. The wavenumbers and energy density are normalized by the grid wavenumber and the averaged subgrid-scale energy dissipation ($-\langle \overline{S}_{ij}\tau_{ij}\rangle$). Figure 10(*b*) is premultiplied by $k^{5/3}$. In these 'mesh-Kolmogorov units', one expects simulations with different meshes to collapse at high wavenumbers, and the spectra to follow the universal power law in the inertial range. The dotted line in figure 10(*a*) shows a power law $(k/k_\Delta)^{-5/3}$. A slight decay below the power law for $k/k_\Delta > 0.3$ and a 'pile-up' very close to the cutoff wavenumber k_Δ are visible. These are known effects of physical-space eddy-viscosity closures, which do not have a 'cusp' near k_Δ (Kraichnan, 1976). These defects appear not to be remedied by the dynamic model in its Lagrangian implementation. We have confirmed that the same is true for the traditional dynamic model by running the same program with the volume-averaged dynamic coefficient.

With regard to computational cost, we find that the CPU time for the simulation with the Lagrangian averaging was higher by about 9% than that of the volume-averaged dynamic model. Most of the additional time was spent in the linear interpolations. Two additional scalar arrays had to be defined, for $\mathcal{I}_{LM}$ and $\mathcal{I}_{MM}$. Compared to overall memory requirements, this addition was not significant.

4.2. *Decaying isotropic turbulence*

In order to test the model in an unsteady case, we perform LES of decaying isotropic turbulence and compare the results with the experimental data of Comte-Bellot & Corrsin (1971). The initial three-dimensional energy spectrum is made to match the

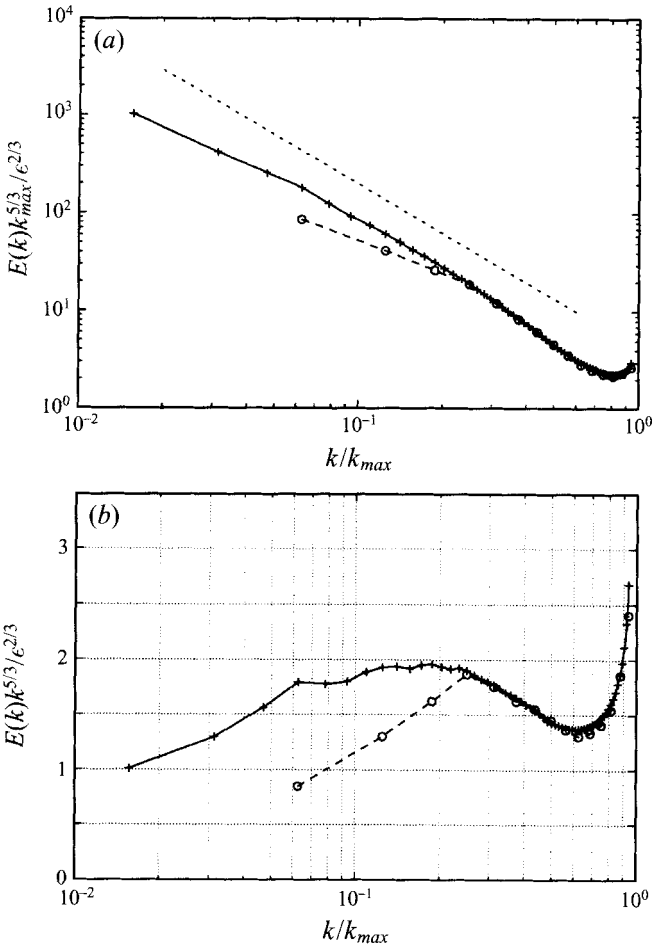

FIGURE 10. Radial energy spectra of LES using the Lagrangian dynamic Smagorinsky model at $Re = \infty$. Wavenumbers are scaled with the grid wavenumber while the energy density is scaled on the grid wavenumber as well as the mean subgrid-scale energy dissipation rate, $\epsilon = -\langle \tau_{ij}\bar{S}_{ij}\rangle$. (*a*) Conventional spectra, (*b*) premultiplied spectra: ——— , 128^3 simulation; - - - - , 32^3 run; ····· , slope $-5/3$. 32^3 spectrum averaged over 240 independent samples taken from 15000 time steps (approximately 13 integral large-scale turnover times L/u', with $L = 2\pi$). The 128^3 spectrum is based on 290 samples taken from 6000 timesteps (approximately 4 large-scale turnover times).

experimental measurements at their earliest time. The phase of the Fourier coefficients is chosen to be random so that the initial velocity field has Gaussian statistics. The dimension of the computational box is chosen to be roughly 4 integral scales.

Figure 11 shows the decay of the kinetic energy compared with the experimental results of Comte-Bellot & Corrsin (1971). The predicted initial decay appears to be a little slower than the experimental rate, but the overall agreement is good. Of course the agreement could have been improved by using a slightly larger value of $c_s^2(0)$ as initial condition – an after-the-fact adjustment that we opted to avoid. A comparison of the spectra at the three different times at which experimental results are available is shown in figure 12. The decrease in overall kinetic energy and the decrease of k at which the spectra peak (increasing integral scale) is clearly reproduced well.

We conclude that the model is able to reproduce important features of this time-dependent flow.

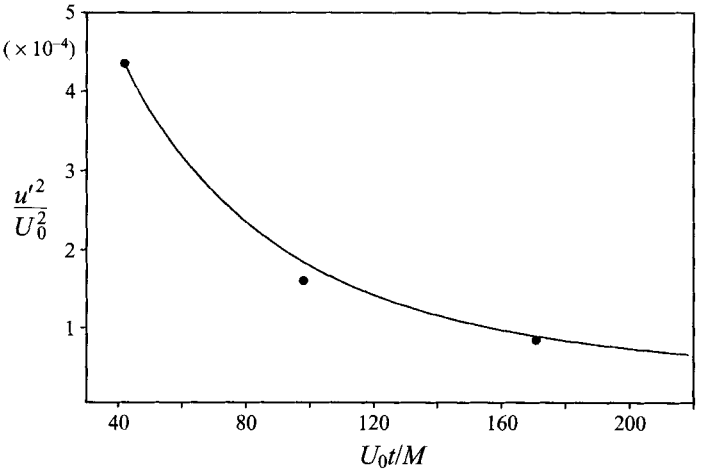

FIGURE 11. Temporal decay of turbulent kinetic energy in isotropic turbulence: ——— , 32^3 LES using the Lagrangian dynamic model; • , filtered experimental results (Comte-Bellot & Corrsin 1971). U_0 and M are the mean fluid speed and the spacing of the turbulence-generating grid in the experiment.

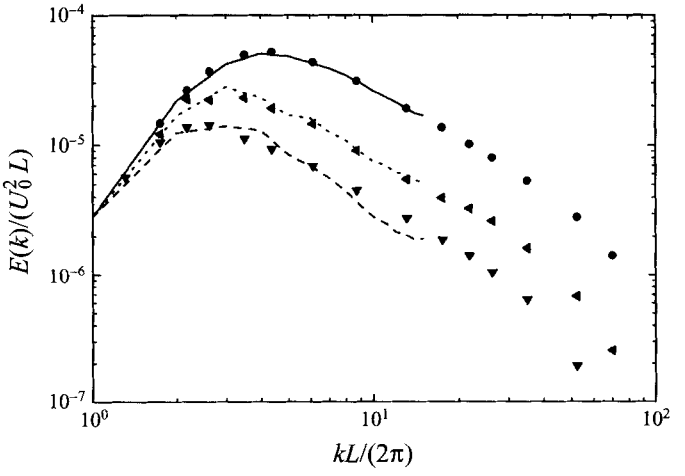

FIGURE 12. Radial energy spectra for decaying isotropic turbulence at different times: lines: 32^3 LES with the Lagrangian dynamic model; solid, dotted and dashed curves: $U_0 t/M = 42$, 98 and 171 respectively. Solid symbols: experimental results of Comte-Bellot & Corrsin (1971) at the same time. U_0 and M are defined in figure 11. $L = 10.8M$ is the computational box size.

4.3. *Fully developed channel flow*

In this section we describe the application of the Lagrangian dynamic model to a pseudo-spectral simulation of plane channel flow. For comparison, another LES is performed with the traditional implementation of the dynamic model in which the terms are averaged over planes parallel to the wall. The flow Reynolds number is selected to match the experimental data by Hussain & Reynolds (1970) to permit detailed comparison.

The channel flow simulations are performed with a pseudo-spectral code (Kim, Moin & Moser 1987) in a numerical domain with streamwise, wall-normal, and spanwise dimensions of $3\pi \times 2 \times 3\pi/4$ (in units of channel half-width d) on a

$48 \times 65 \times 64$ mesh. Chebyshev polynomials are used in the wall-normal direction on a collocated grid; Fourier transforms are used in the homogeneous streamwise and spanwise directions on a uniform grid. Real-space (tophat) filtering is used for the dynamic test filtering procedure and is performed explicitly only in horizontal planes. The equivalent filter width Δ_{eq} is taken to be the geometric mean of unidirectional grid widths (this procedure is justified for moderate grid anisotropies, as shown in Scotti, Meneveau & Lilly 1993). For the plane-averaged LES, averaging of the dynamic coefficient is performed in horizontal planes.

The approximate Lagrangian interpolation for the horizontal directions is implemented in this code as described in §3.3. The wall-normal direction requires different treatment due to the stretched mesh used in that direction. The transformation $\theta = \cos^{-1}(y/d)$ is used to map the stretched mesh into a uniform one. The wall-normal advection term, $v\partial/\partial y$, is recast as $v_\theta \partial/\partial\theta$ and the interpolation is performed in θ identically to the horizontal directions, but using $v_\theta = -v/\sin\theta$. The wall planes are treated specially with $\mathcal{I}_{LM} \equiv 0$ and $\mathcal{I}_{MM}$ approximated by values at the nearest off-wall plane. There was also the possibility that the interpolation might attempt to place approximated points at the previous time step beyond the walls; however, the explicit time-step stability restriction gives sufficiently small time steps that this situation is never encountered.

A target friction Reynolds number Re_τ ($\equiv u_\tau d/\nu$, where the friction speed u_τ is the square root of the mean total wall stress, d is the channel half-width, and ν is the molecular viscosity) of 650 was chosen, corresponding to one set of experimental data by Hussain & Reynolds (1970). The channel flow is started from a flow field at lower Reynolds number and is allowed to evolve to near statistical equilibrium, with $Re_\tau \approx 641$ in the last runs. The initial conditions for $\mathcal{I}_{LM}$ and $\mathcal{I}_{MM}$ are chosen as in the homogeneous case but with $c_s^2(0)$ as function of y matching the values of a previous plane-averaged dynamic simulation. Using the Lagrangian formulation proved to be more expensive than the standard plane-averaged method by roughly 10%, in part due to the need to perform a division at each point to compute the dynamic coefficient rather than at each plane. The Lagrangian method also requires extra mass storage of $\mathcal{I}_{LM}$ and $\mathcal{I}_{MM}$ between runs.

The averaged statistics will be shown first, followed by a more detailed analysis of additional variables.

Figure 13 shows the mean velocity profile in the half-channel, in outer units (*a*) and wall units (*b*). As can be seen, at the resolution of the present LES, the plane-averaged model overpredicts the centreline velocity (smaller losses) for the prescribed pressure gradient. In the buffer layer, the velocity predicted by the Lagrangian model is slightly below the measured values. However the magnitude of the error is considerably smaller than that of the plane-averaged case, and elsewhere the agreement is good. Figure 14 shows the profiles of *r.m.s.* velocities and Reynolds shear stress of the resolved fields, and a comparison of the *r.m.s.* streamwise velocity with the measurements of Hussain & Reynolds (1970). In the core region (for $y/d > 0.2$), the LES with both models fall slightly below the measured values. Closer to the wall, both LES overpredict u_{rms}, but the Lagrangian model does a better job than the plane-averaged one.

The mean eddy viscosity predicted by both LES is shown in figure 15. It is computed according to

$$\langle \nu_t \rangle(y) = \langle c_s^2(x, y, z, t)\ \Delta_{eq}^2 |\overline{S}| \rangle_{x,z,t}, \tag{4.1}$$

where the averaging is performed over (x, z) planes and time. The coefficient c_s^2 is

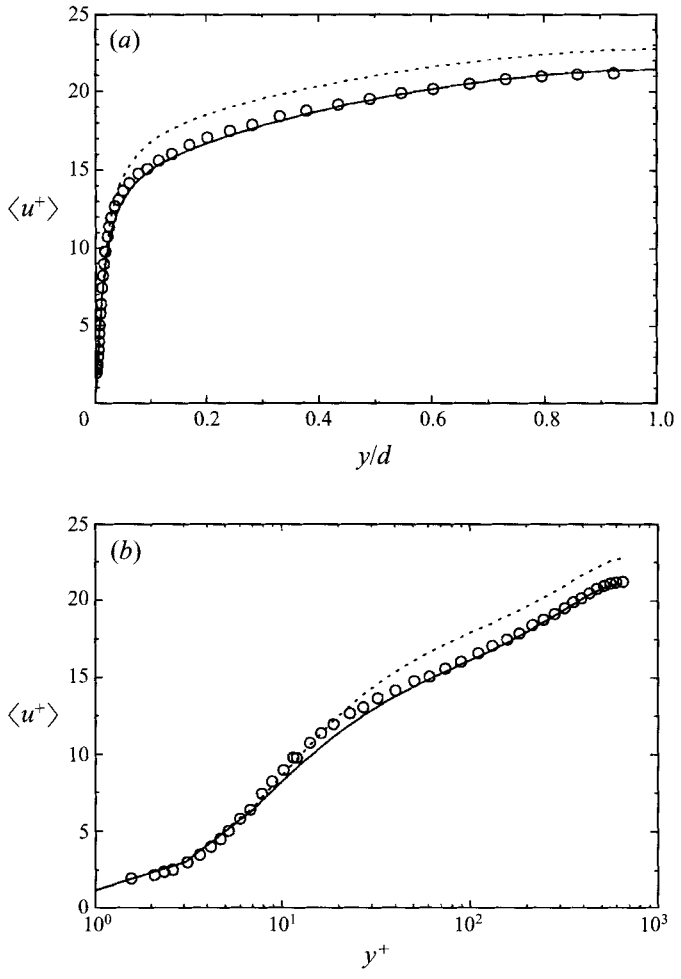

FIGURE 13. Mean velocity profiles in fully developed channel flow: ····· , LES with the plane-averaged dynamic model; ——— , LES with the Lagrangian dynamic model; ○ : Experimental measurements of Hussain & Reynolds (1970). (*a*) Wall distance in units of the half-channel width *d*, (*b*) in wall units.

computed according to either the plane-averaged or the Lagrangian dynamic model. It can be seen that over much of the log-layer, the Lagrangian model generates a lower eddy viscosity than the plane-averaged dynamic model. We have checked that this reduction is due primarily to a decrease in the dynamic coefficient c_s^2 as opposed to reduced strain-rate magnitudes. Figure 15(*b*) shows that the reduced eddy viscosity in the case of the Lagrangian model results in less SGS dissipation which in turn is probably the cause for the increased resolved shear stress observed before. Figure 15(*b*) also indicates that, on a local basis, both models contribute more than 50% of the total dissipation rate over much of the channel. This is significant since it indicates that the subgrid-scale model plays a key role in the resolved-scale turbulence energy budget.

An important feature of the original dynamic model is that it exhibits the proper near-wall scaling for the SGS eddy viscosity when the sublayer is numerically resolved (Germano *et al.* 1991), namely $\nu_t \sim (y^+)^3$. As can be seen in figure 15(*a*), this scaling is

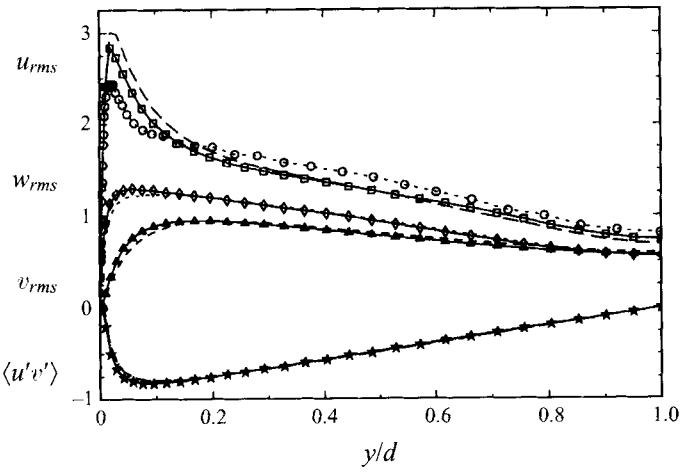

FIGURE 14. Profiles of second-order moments of the resolved velocity field: ---- , u_{rms} from the plane-averaged LES; □ , u_{rms} from the Lagrangian model; ○ , u_{rms} from the experimental measurements of Hussain & Reynolds (1970). ◇ , Spanwise w_{rms} from Lagrangian LES; ····· , from the plane-averaged model. △ , Wall-normal v_{rms} from Lagrangian LES; - - - - , from the plane-averaged model. ⋆, Resolved shear stress $\langle u'v' \rangle$ from Lagrangian LES; —·— , from the plane-averaged model.

followed quite well by the plane-averaged case (as observed before by Germano *et al.* 1991; Piomelli 1993). The Lagrangian model deviates slightly, producing a near-wall distribution that is closer to $\nu_t \sim (y^+)^{2.9}$. We shall comment on this small discrepancy later in this section. For now, we simply note that the deviation in slope is rather small and that its manifestation is limited to an increase of the eddy viscosity in the viscous sublayer. The eddy viscosity is one to four orders of magnitude smaller than the molecular viscosity in this region, however, and it seems unlikely that differences at this level could have a measurable impact on the computed results.

With the purpose of documenting the statistics of the model coefficient c_s^2 and its evolution away from the initial condition, we show in figure 16(*a–c*) probability density functions of c_s^2 at different times and different elevations from the wall. The p.d.f. at $t = 0$ is a *delta*-function at the plane-averaged value of the dynamic coefficient, which is used as initial condition. As can be seen, the convergence of the p.d.f. to the asymptotic value (circles) is nearly complete after 80 time steps. This duration corresponds to about $\nu/u_\tau^2 \sim 25$ viscous times or $d/u_\tau \sim 0.04$ outer times. Figures 16(*b*) and 16(*c*) clearly show the considerable decrease of typical c_s^2 values in the Lagrangian model as compared to the plane-averaged model.

The main issue left to answer is why the Lagrangian model generates such decreased coefficients in the log-layer. For this purpose, the average values of numerators and denominators are evaluated separately for both models on some sample planes as given in table 1.

The largest discrepancy can be seen by comparing the denominators $\langle M_{ij}M_{ij} \rangle$ and $\langle \mathscr{I}_{MM} \rangle$ at $y^+ = 108$. A possible reason for this discrepancy can be deduced by comparing $\langle M_{ij}M_{ij} \rangle$ at $y^+ = 12$ and at $y^+ = 108$. $\langle M_{ij}M_{ij} \rangle$ and $\langle \mathscr{I}_{MM} \rangle$ are several orders of magnitude higher in the near-wall region, as is to be expected for a variable based on the strain rate (to the fourth power). During ejection events, fluid particles that were close to the wall reach deep into the log-layer, thus convecting elevated values of $\mathscr{I}_{MM}$ upwards. This feature can be deduced from figure 17, which shows

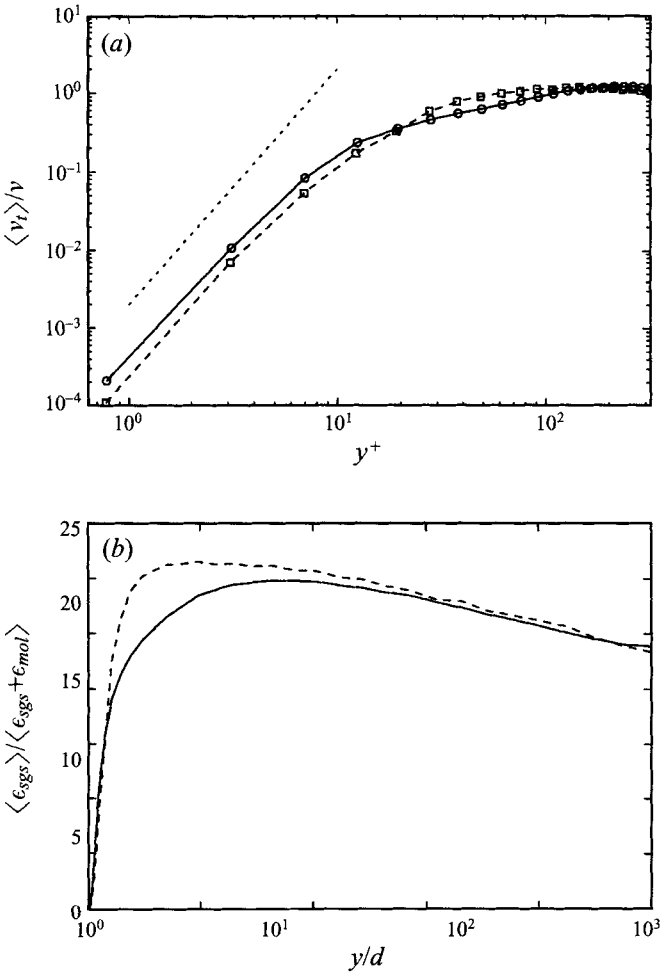

FIGURE 15. (*a*) Ratio of plane-averaged eddy viscosity to molecular viscosity taken from the channel flow simulation. ○ , Lagrangian dynamic model; □ , plane-averaged dynamic model; ····· , $\nu_t \sim (y^+)^3$ power-law. (*b*) Ratio of plane-averaged SGS dissipation rate to plane-averaged total (SGS + molecular) dissipation rate. ——— , Lagrangian; - - - - , plane-averaged dynamic model.

LES – plane-averaged			
y^+	12	108	640
$\langle L_{ij} M_{ij} \rangle$	9.819×10^1	3.632	0.1102
$\langle M_{ij} M_{ij} \rangle$	1.030×10^5	3.341×10^2	7.015

LES – local Lagrangian			
y^+	12	108	641
$\langle \mathscr{I}_{LM} \rangle$	9.464×10^1	4.186	0.1071
$\langle \mathscr{I}_{MM} \rangle$	1.549×10^5	6.090×10^2	8.917

TABLE 1. Numerators and denominators in the expressions for the dynamic coefficients averaged over sample planes.

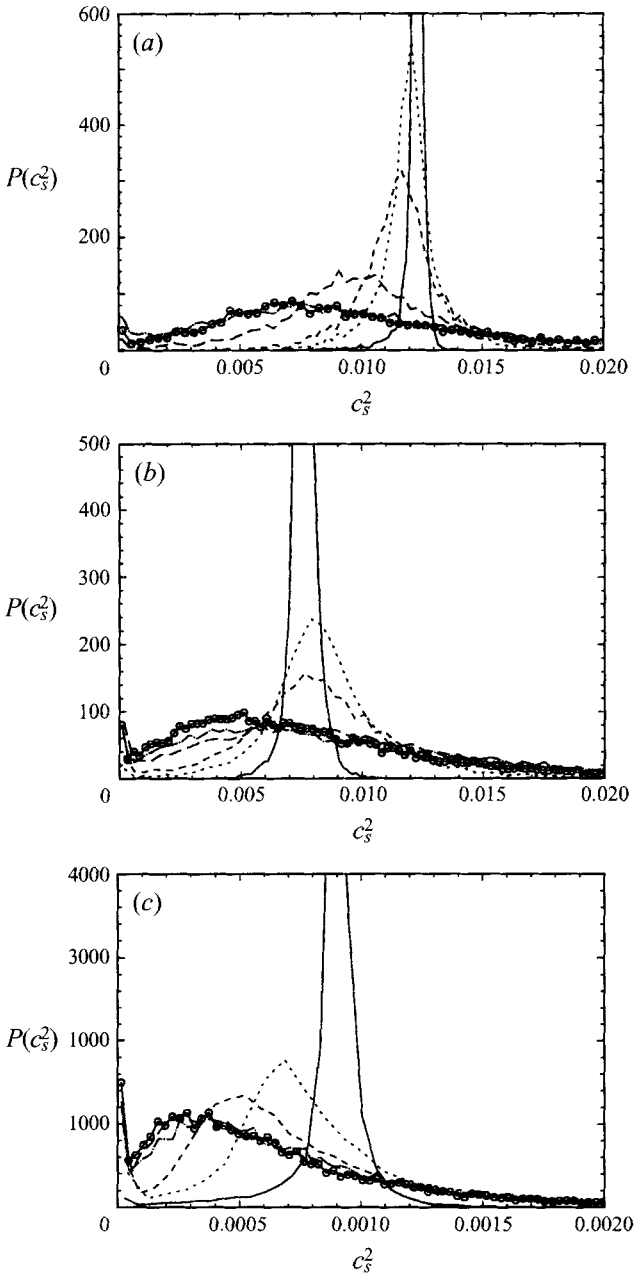

FIGURE 16. Probability density functions of dynamic model coefficient c_s^2 for different time steps, n: ——— , $n = 2$; ····· , $n = 10$; - - - - , $n = 20$; — — — , $n = 80$; — — — , $n = 320$; —·— , $n = 640$; ○ , $n \sim 5 \times 10^4$. Different graphs are at different heights above the wall: (*a*) $y^+ = 641$, (*b*) $y^+ = 108$ and (*c*) $y^+ = 12$.

a scatter plot of the Lagrangian denominator $\mathscr{I}_{MM}$ as function of the local vertical velocity. Clearly, large values of $\mathscr{I}_{MM}$ are associated with positive values of v', which are indicative of ejection events.

The net effect is that the Lagrangian model is less dissipative as far as ejection events are concerned. They can survive longer and feed more turbulence into the

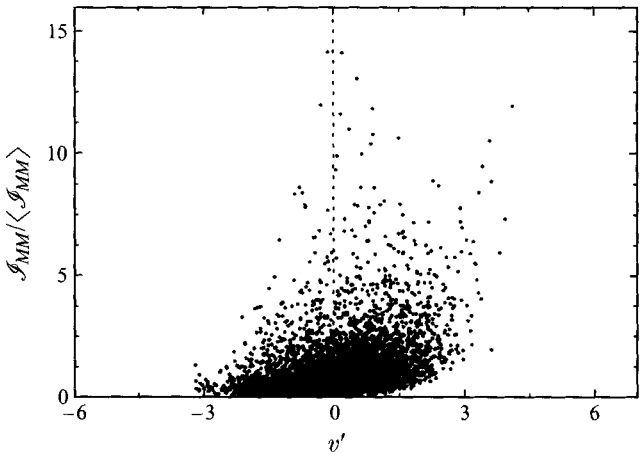

FIGURE 17. Scatter plot of $\mathscr{I}_{MM}$ versus vertical velocity v' in LES of channel flow, using the Lagrangian dynamic model.

channel flow, producing more realistic (higher) levels of Reynolds-averaged (resolved) eddy viscosity and losses than the plane-averaged case.

It is likely that a similar phenomenon causes the near-wall scaling of Lagrangian eddy viscosity to be less steep than that of the plane-averaged model. Occasionally, 'sweeps' bring log-layer material into the sublayer and effectively increase the model coefficient and eddy viscosity above that of the plane-averaged model. Numerical diffusion is also likely to play a role in reducing spatial differences in $\mathscr{I}_{LM}$ and $\mathscr{I}_{MM}$.

As mentioned in §3.2, some arbitrariness is involved in selecting the time scale for the Lagrangian average. This time scale, T, is controlled by the parameter θ in (3.11). An important question is whether the LES results are sensitive to changes in θ. We have seen that Lagrangian averaging in channel flow has a considerable impact on the simulation due to the spatial non-homogeneity, and we may therefore expect some variation in the computed statistics with variations in θ. We have made an attempt to quantify the sensitivity to the parameter θ by performing two additional channel flow simulations: one where the time scale was decreased by a factor of two ($\theta = 0.75$) and another where the time scale was increased by a factor of two ($\theta = 3$). (The simulation discussed previously was run with $\theta = 1.5$.) The results are shown in figures 18(a) and 18(b) where the mean velocity, r.m.s., and shear-stress profiles are plotted. As can be seen, there indeed is an impact of the time scale on the final results, more so in the mean velocity profiles than in the second-order moments. The differences are not particularly large however, and all three choices of the time scale yield results that are closer to the experimental results of Hussain & Reynolds than the plane-averaged case. The trends follow what is expected on intuitive grounds: as the time-scale becomes small, the model becomes more local and more dissipative (higher mean viscosity); for very large time scales, the averaging encompasses a large volume, including regions (too) close to the wall, which yields smaller coefficients and generates less SGS dissipation, leading to higher shear stresses and thus to lower mean velocity. In summary, we have documented the sensitivity of the simulation within a reasonable range of values for the free parameter θ. We have found that some sensitivity exists, but that it is not unreasonably large (for further discussion of this issue see §5).

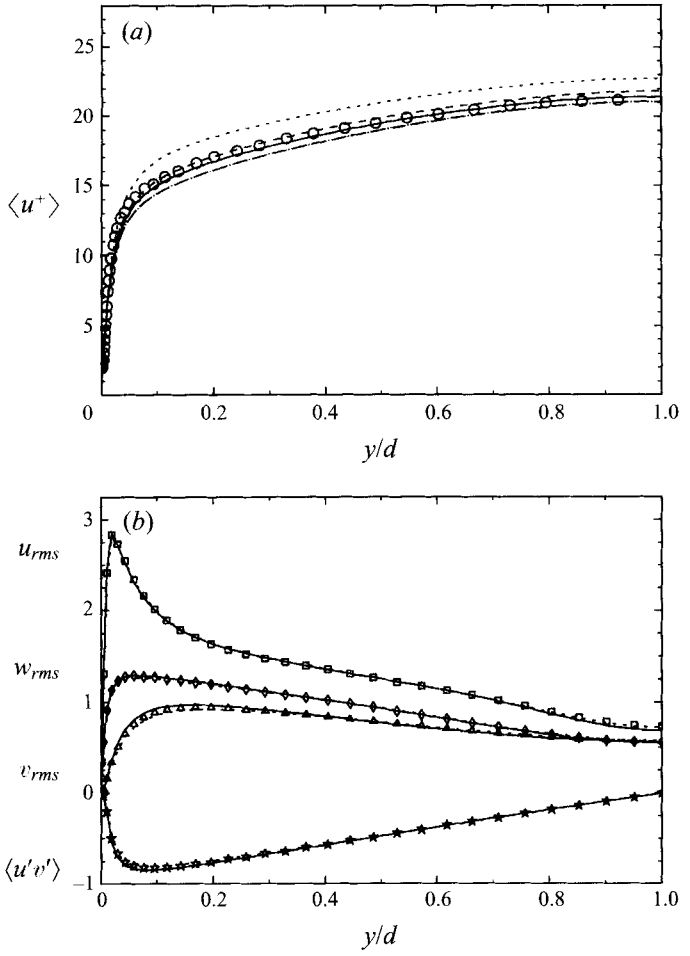

FIGURE 18. Impact of Lagrangian averaging time scale on mean profiles in fully developed channel flow. (*a*) Mean velocity profiles: ····· , LES with the plane-averaged dynamic model; – – – – , LES with the Lagrangian model, $\theta = 0.75$; ——— , LES with the Lagrangian model, $\theta = 1.5$; —·— , LES with the Lagrangian model, $\theta = 3$; ○ , experimental measurements of Hussain & Reynolds (1970). (*b*) Second-order moments of the resolved velocity field. Symbols (Lagrangian model with $\theta = 1.5$: □ , streamwise u_{rms}; ◇ , spanwise w_{rms}; △ , wall-normal v_{rms}; ⋆, resolved shear stress $\langle u'v' \rangle$. – – – – , Same as symbols but with $\theta = 0.75$; ——— , same as symbols but with $\theta = 3$.

4.4. *Transitional channel flow*

A known drawback of the traditional eddy viscosity closure for LES of transitional flows is that it is overly dissipative, possibly eliminating instabilities altogether (Piomelli & Zang 1991). The dynamic model, on the other hand, yields essentially zero eddy viscosity if the resolved part of the flow is not turbulent. Instabilities are thus allowed to grow initially in a realistic fashion, as shown in simulations of transitional channel flow using the dynamic model, with planar averaging (Germano *et al.* 1991). Once the nonlinear breakdown phase is reached, the SGS model must become active in order to prevent excessive growth of turbulent kinetic energy, wall shear stresses, etc. In the Lagrangian model, the variable $\mathcal{I}_{LM}$ must be initialized to zero everywhere in the laminar region. As turbulence is generated, this variable (and therefore the eddy viscosity) will rise from zero. The rate at which $\mathcal{I}_{LM}$ rises from zero is controlled

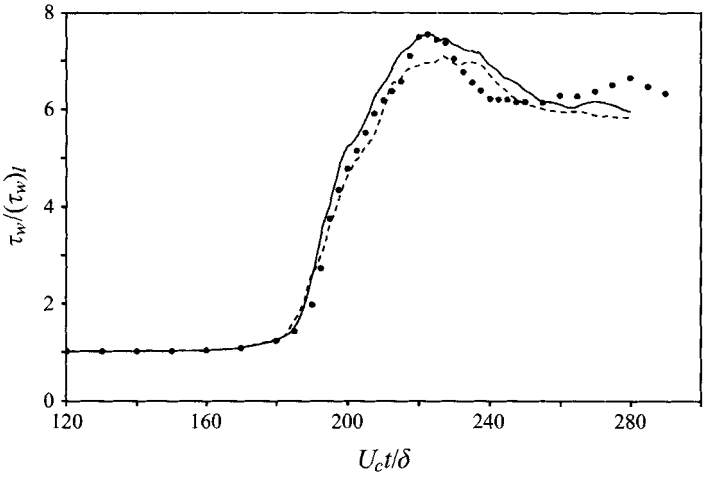

FIGURE 19. Time history of wall shear stress from the transitional channel simulation: ——— , Lagrangian model LES; - - - - , plane-averaged dynamic model LES; • , DNS of Zang *et al.* (1990).

in part by the memory time scale. If the memory time scale, T, is too long, the rise in eddy viscosity may occur too late in the transition process. In order to investigate this potential problem, we have performed an LES of transitional channel flow. In this section we attempt to ascertain if the Lagrangian model as proposed here (with the time scale given by (3.11)) is able to (i) allow for initial instabilities to grow in a realistic fashion, and then to (ii) sufficiently damp the turbulence at the appropriate time.

The transition channel case is identical to that of Zang, Gilber & Kleiser (1990), Piomelli & Zang (1991) and Germano *et al.* (1991). The initial (laminar) centre-line Reynolds number is 8000. The initial condition consists of a parabolic mean flow plus a two-dimensional Tollmien–Schlichting wave of 2% amplitude and a pair of three-dimensional Tollmien–Schlichting waves of 0.02% amplitude. The streamwise wavenumber for both the two-dimensional and three-dimensional modes is 1.0, whereas the spanwise wavenumber for the three-dimensional modes is ± 1.5. See Zang *et al.* (1990) for more details on the initial conditions. The dimensions of the computational domain (streamwise, wall-normal, and spanwise) are $2\pi \times 2 \times 4\pi/3$ (in units of δ). The term $\mathscr{I}_{LM}$ is initialized to 10^{-14} (instead of to zero) in order to allow the first-order Euler scheme (explicit in T^n) to move $\mathscr{I}_{LM}$ away from zero once the source term $L_{ij}M_{ij}$ becomes non-zero.

The calculation is started on a $16 \times 65 \times 16$ mesh. As the transition process proceeds, the solution is interpolated onto increasingly finer meshes. The timings of the remeshings are determined by monitoring the energy content in the highest resolved frequencies in the streamwise and spanwise directions. The remeshing procedure was found to introduce a complication in the Lagrangian SGS model. Refining the mesh while holding the test-to-grid filter ratio fixed results in different values of $L_{ij}M_{ij}$ and $M_{ij}M_{ij}$. Because of its memory, the Lagrangian model requires a finite amount of time to adjust to the sudden changes in $L_{ij}M_{ij}$ and $M_{ij}M_{ij}$ (about $\Delta t = 5$, or 100 time steps). In order to minimize this recovery time, the remeshing is performed with values of $\mathscr{I}_{LM}$ and $\mathscr{I}_{MM}$ rescaled so that their plane-averaged values are equal to those of the instantaneous $L_{ij}M_{ij}$ and $M_{ij}M_{ij}$, respectively. Early in the transition process the SGS dissipation is minuscule and errors associated with

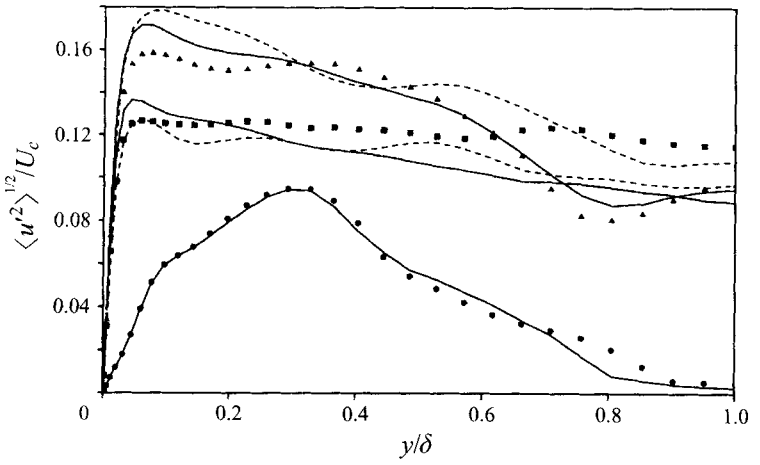

FIGURE 20. Streamwise velocity fluctuation profiles from the transitional channel flow simulation. Symbols: DNS of Zang *et al.* (1990): ●, $t = 176$; ▲, $t = 200$; ■, $t = 220$; ——— . Lagrangian model LES; - - - - , plane-averaged dynamic model LES.

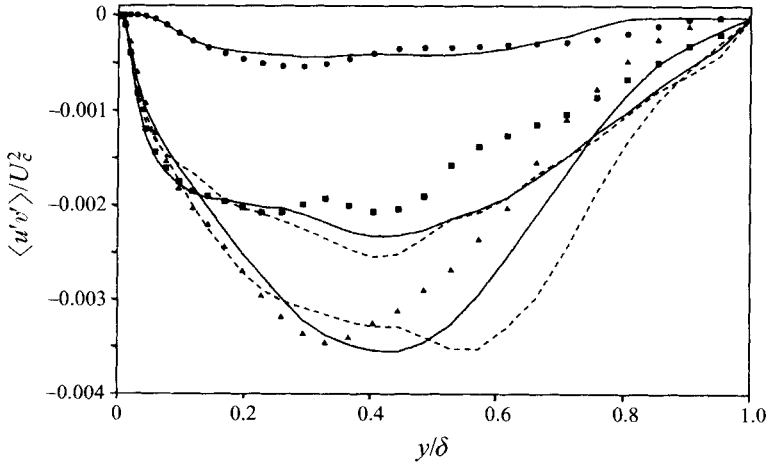

FIGURE 21. Reynolds shear stress profiles from the transitional channel flow simulation. Symbols DNS of Zang *et al.* (1990): ●, $t = 176$; ▲, $t = 200$; ■, $t = 220$. ——— , Lagrangian model LES; - - - - , plane-averaged dynamic model LES.

remeshing probably have a negligible effect. However, the flow may be more sensitive to remeshing at later times when the SGS dissipation is not negligible.

The $16 \times 65 \times 16$ mesh is used until $t = 145$ (in units of initial centreline velocity U_c and δ), when the grid is remeshed to $24 \times 65 \times 24$. The run is then continued to $t = 176$ on both $24 \times 65 \times 24$ and $32 \times 65 \times 32$ meshes (with little notable difference). The field is then remeshed to $32 \times 65 \times 48$. Another remeshing to $48 \times 65 \times 64$ is performed at $t = 200$, and the simulation is then run without further remeshing to $t = 280$.

Figure 19 shows the time history of the wall shear stress compared with the DNS of Zang *et al.* (1990). Results from the plane-averaged dynamic model are included in this figure. The Lagrangian model is in good agreement with the DNS results up to $t = 210$. Then, the wall shear stress slightly overshoots around the peak after

which it settles to a plateau, near the DNS value. The plane-averaged dynamic model results are similar, with the exception that the peak shear stress is underpredicted. Streamwise velocity fluctuations from the Lagrangian and plane-averaged models at times $t = 176$, 200, and 220 are compared with the (filtered) DNS data in figure 20. Overall the agreement is quite good, and at $t = 176$ it is excellent. At this time the Lagrangian and plane-averaged results are indistinguishable. Reynolds shear stresses are shown in figure 21. Very good agreement is obtained at $t = 176$, whereas some differences exist at $t = 200$ and $t = 220$.

Overall these results show that the Lagrangian model is capable of simulating transition. The eddy viscosity does rise from zero with a delay which is small enough so that turbulence is sufficiently damped after the rapid growth of kinetic energy during transition.

5. Summary and conclusions

A new version of the dynamic Smagorinsky model has been developed where the Germano identity is averaged for some time along fluid pathlines rather than over directions of statistical homogeneity, as was common practice in previous applications of the dynamic model. The present method is not restricted to cases with homogeneous directions and is readily applicable to complex-geometry, unsteady flows. We have shown that if an exponential memory is employed, the required averages can be obtained by solving a pair of relaxation-transport equations. In order to allow for the implementation of this model with minimal computational complications, we have proposed discretizing the total derivatives that enter these equations using a first-order expression in time, coupled with linear spatial interpolation to find the values required at the 'upstream' locations. The resulting formulation (embodied in (3.13) and (3.14)) is very simple to implement.

Our approach is motivated, in part, by the idea that the Smagorinsky parameterization is appropriate in an average rather than a local sense. Averaging used in conjunction with the dynamic model introduces a statistical element that helps to return the Smagorinsky parameterization to a more solid foundation. Existing spatial averaging schemes are effective in this regard, but require one or more homogeneous directions. Averaging along particle trajectories also introduces a statistical element, but has the distinct advantage that it is applicable in inhomogeneous flows. Furthermore, while spatially averaged schemes remove all variations in the homogeneous directions, a Lagrangian average preserves a certain degree of locality in space. High-frequency, point-to-point oscillations are eliminated in the Lagrangian model, whereas statistically significant large-scale variations in subgrid-scale activity can be captured. Tests in LES of isotropic turbulence showed that spatial variations present in the coefficient field are indeed correlated with the dominant structures in that flow ('fat worms').

The effects of averaging have been investigated in DNS and LES of forced isotropic turbulence. *A priori* tests using DNS showed that averaging over a few small-scale turn-over times significantly reduces the coefficient scatter. For smooth filters (in Fourier space) such as the Gaussian and tophat, such averaging greatly increases the correlation between coefficients at two scales. This effect is much weaker when a sharp cutoff filter is used, however, and the correlation remains low even after averaging. Since the LES of isotropic turbulence performed here use cutoff test filtering, the simulations may not benefit from an increased correlation among the coefficients at the test and grid levels as a result of the Lagrangian average. However, the coefficient variance is reduced as a result of the Lagrangian average even with the cutoff filter

and this feature allows a numerically stable model that is able to capture large-scale variations in the coefficient field.

The effect of the Lagrangian averaging on the p.d.f.s of various quantities involved in the model was also studied. Lagrangian averaging with a time scale that depends on the numerator itself was shown to produce a non-negative distribution for the numerator, and to eliminate the probability of vanishingly small denominators. The p.d.f. of the model coefficient was also observed to be non-negative and more strongly concentrated around its mean value.

Applications of the Lagrangian model to LES of isotropic turbulence and fully developed and transitional channel flow have shown that it performs well. Comparisons with the spatially averaged dynamic model indicate that the Lagrangian model is equally accurate in isotropic turbulence and slightly superior in channel flow. The increased accuracy in the latter case was attributed to a reduction of eddy viscosity in the buffer layer which results from tracking ejection events that transport near-wall information into the outer region. Good results were also obtained in transitional channel flow, indicating that the averaging time is short enough to allow the model to respond to unsteady phenomena.

While we have presented evidence to suggest that averaging is beneficial in the dynamic model formulation, we recognize that generally applicable purely local formulations are also possible, such as those of Ghosal *et al.* (1995), and Piomelli & Liu (1995). Interestingly, both Piomelli & Liu (1995) and Ghosal *et al.* (1995) obtained slightly more accurate results with the local models than with models that average the equations over homogeneous directions. The fact that our model is also slightly more accurate than the spatially-averaged versions suggests that spatial variability of the coefficient field may, in general, lead to improved results. What is not clear, however, is how much spatial variation is required. Our results would seem to suggest that spatial variations at a scale of the dominant flow structures are sufficient.

Although we have focused exclusively on the Smagorinsky model in this work, we reiterate that the Lagrangian averaging procedure can be used in conjunction with other subgrid-scale parameterizations. Alternative base models may add improved physical description of the subgrid-scale motions and averaging along fluid trajectories will add a statistical element, whenever this is deemed desirable.

Finally, it is important to recognize that the Lagrangian dynamic model contains some arbitrary elements, in particular an adjustable memory time scale T. This fact is unfortunate since it appears to conflict with the dynamic model philosophy of dispensing with adjustable parameters in favour of determining the subgrid-scale stress solely from information contained in the resolved velocity field. However, for any implementation that uses spatial averaging, there is a similar need for choosing, *a priori*, the extent of the domain over which Germano's identity is to be enforced. At any rate, the sensitivity of the simulations to T was found to be acceptably small.

The authors have benefited from fruitful discussions with Professors Parviz Moin and Javier Jimenez, and Dr Sandip Ghosal, and they thank Professor Ugo Piomelli for his detailed comments on an earlier version of this manuscript. They also thank Mr Anh-Tuan Le and Dr Gary Coleman for their careful checking of model implementation in the channel flow code. This work was initiated at CTR during the 1994 Summer Program. C.M. gratefully acknowledges this support from CTR, as well as support from ONR (grant N-00014-92-J-1109, monitored by Dr P. Purtell). T.S.L. acknowledges partial support from the ONR (grant N-00014-91-J-4072) and from the AFOSR (grant F49620-92-J0003).

REFERENCES

Akselvoll, K. & Moin, P. 1993 Application of the dynamic localization model to large-eddy simulation of turbulent flow over a backward-facing step. In *Engineering Applications to Large-Eddy Simulation* (ed. U. Piomelli & S. Ragab), pp. 1–6. ASME.

Bardina, J., Ferziger, J. H. & Reynolds, W. C. 1980 Improved subgrid scale models for large eddy simulation. *AIAA Paper* 80-1357.

Briscolini, M. & Santangelo, P. 1994 The non-Gaussian statistics of the velocity field in low-resolution large-eddy simulation of homogeneous turbulence. *J. Fluid Mech.* **270**, 199–217.

Carati, D., Ghosal, S. & Moin, P. 1995 On the representation of backscatter in dynamic localization models. *Phys. Fluids* **7**, 606–616.

Chasnov, J. R. 1991 Simulation of the Kolmogorov inertial subrange using an improved subgrid model. *Phys. Fluids* A **3**, 188–200.

Chollet, J. P. & Lesieur, M. 1981 Parameterization of small scales of three-dimensional isotropic turbulence utilizing spectral closures. *J. Atmos. Sci.* **38**, 2747–2757.

Clark, R. A., Ferziger, J. H. & Reynolds, W. C. 1979 Evaluation of subgrid-scale turbulence models using an accurately simulated turbulent flow. *J. Fluid Mech.* **91**, 1–16.

Comte-Bellot, G. & Corrsin, S. 1971 Simple Eulerian time correlation in full and narrow band velocity signals in grid generated, isotropic turbulence. *J. Fluid Mech.* **48**, 273–337.

Germano, M., Piomelli, U., Moin, P. & Cabot, W. H. 1991 A dynamic subgrid-scale eddy viscosity model. *Phys. Fluids* A **3**, 1760–1765.

Ghosal, S., Lund, T. S., Moin, P. & Akselvoll, K. 1995 A dynamic localization model for large-eddy simulation of turbulent flow. *J. Fluid Mech.* **286**, 229–255.

Hussain, A. K. M. F. & Reynolds, W. C. 1970 The mechanics of a perturbation wave in turbulent shear flow. *Stanford Univ. Dept. of Mech. Eng. Rep.* FM-6.

Jimenez, J., Wray, A. A., Saffman, P. G. & Rogallo, R. S. 1993 The structure of intense vorticity in isotropic turbulence. *J. Fluid Mech.* **255**, 65–90.

Kim, J., Moin, P. & Moser, R. 1987 Turbulence statistics in fully developed channel flow at low Reynolds number. *J. Fluid Mech.* **177**, 133–166.

Kraichnan, R. H. 1976 Eddy viscosity in two and three dimensions. *J. Atmos. Sci.* **33**, 1521–1576.

Leith, C. 1990 Stochastic backscatter in a subgrid-scale model: plane shear mixing layer. *Phys. Fluids* A **2**, 297–299.

Leslie, D. C. & Quarini, G. L. 1979 The application of turbulence theory to the formulation of subgrid modelling procedures. *J. Fluid Mech.* **91**, 65–91.

Lilly, D. K. 1967 The representation of small-scale turbulence in numerical simulation experiments. In *Proc. IBM Sci. Comput. Symp. on Environmental Sciences*, IBM Form No. 320-1951, pp. 195–210.

Lilly, D. K. 1992 A proposed modification of the Germano subgrid-scale closure method *Phys. Fluids* A **4**, 633–635.

Liu, S., Meneveau, C. & Katz, J. 1994 On the properties of similarity subgrid-scale models as deduced from measurements in a turbulent jet. *J. Fluid Mech.* **275**, 83–119.

Liu, S., Meneveau, C. & Katz, J. 1995 Experimental study of similarity SGS models of turbulence in the far-field of a jet. *Appl. Sci. Res.* **54** 177–190.

Lund, T. S., Ghosal, S & Moin, P. 1993 Numerical experiments with highly-variable eddy viscosity models. In *Engineering Applications to Large-Eddy Simulation* (ed. U. Piomelli & S. Ragab), pp. 7–11.

Lund, T. S. & Novikov, E. A. 1992 Parameterization of subgrid-scale stress by the velocity gradient tensor. In *Annual Research Briefs, Center for Turbulence Research, Stanford University*, pp. 27–43.

Mason, P. & Thomson, D. 1992 Stochastic backscatter in large-eddy simulations of boundary layers. *J. Fluid Mech.* **242**, 51–78.

McMillan, O. J. & Ferziger, J. H. 1979 Direct testing of subgrid-scale models. *AIAA J.* **17**, 1340–1346.

Meneveau, C. 1994 Statistics of turbulence subgrid-scale stresses: Necessary conditions and experimental tests. *Phys. Fluids* **6**, 815–833.

Meneveau, C. & Lund, T. S. 1994 On the Lagrangian nature of the turbulence energy cascade. *Phys. Fluids* **6**, 2820–2825.

MENEVEAU, C., LUND, T. S. & MOIN, P. 1992 Search for subgrid scale parameterization by projection pursuit regression. In *Proc. Summer Program 1992 Stanford University*, vol IV, pp. 61–81.

MOIN, P. 1991 A new approach for large eddy simulation of turbulence and scalar transport. In *New Approaches and Concepts in Turbulence, Proc. Monte Verita Coll. on Turbulence* (ed. T. Dracos & A. Tsinober). Birkhauser, Bale.

MORRIS, P. & FERZIGER, J. H. 1994 The 2-4 dynamic model for large-eddy simulations (Abstract only). *Bull. Am. Phys. Soc.* **39**, 1896.

PIOMELLI, U. 1993 High Reynolds number calculations using the dynamic subgrid-scale stress model. *Phys. Fluids* A **5**, 1484–1490.

PIOMELLI, U. & LIU, J. 1995 Large-eddy simulation of rotating channel flows using a localized dynamic model. *Phys. Fluids* **7**, 839–848.

PIOMELLI, U. & ZANG, T. A. 1991 Large-eddy simulation of transitional channel flow. *Comp. Phys. Commun.* **65**, 224–230.

ROGALLO, R. 1981 Numerical experiments in homogeneous turbulence. *NASA Tech. Memo* 81315.

SCHUMANN, U. 1995 Stochastic backscatter of turbulence energy and scaler variance by random subgrid-scale fluxes. *Proc. R. Soc. Lond.* A **451**, 293–318.

SCOTTI, A., MENEVEAU, C. & LILLY, D. K. 1993 Generalized Smagorinsky model for anisotropic grids. *Phys. Fluids* A **5**, 2306–2308.

VINCENT, A. & MENEGUZZI, M. 1991 The spatial structure and statistical properties of homogeneous turbulence. *J. Fluid Mech.* **225**, 1–20.

WANG, Q. & SQUIRES, K. D. 1996 Large-eddy simulation of particle-laden turbulent channel flow. *Phys. Fluids* **8**, 1207–1223.

WU, X. & SQUIRES, K. D. 1995 Large eddy simulation of a canonical three-dimensional boundary layer. In *Proc. Tenth Symp. on Turbulent Shear Flows, Penn State* (ed. F. Durst, B. E. Launder, F. W. Schmidt & J. W. Whitelaw).

ZANG, T. A., GILBERT, N. & KLEISER, L. 1990 Direct numerical simulation of the transitional zone. In *Instability and Transition* (ed M. Y. Hussaini & R. G. Voigt), pp. 283–299.

ZANG, Y., STREET, R. L. & KOSEFF, J. 1993 A dynamic mixed subgrid-scale model and its application to turbulent recirculating flows. *Phys. Fluids* A **5**, 3186–3196.

https://doi.org/10.1017/S0022112096007379 Published online by Cambridge University Press